Journal Pre-proof

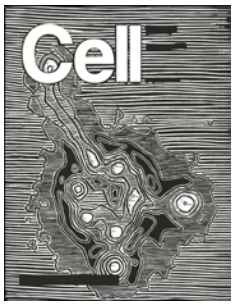

Antibody escape of SARS-CoV-2 Omicron BA.4 and BA.5 from vaccine and BA.1 serum

Aekkachai Tuekprakhon, Jiandong Huo, Rungtiwa Nutalai, Aiste Dijokaite-Guraliuc, Daming Zhou, Helen M. Ginn, Muneeswaran Selvaraj, Chang Liu, Alexander J. Mentzer, Piyada Supasa, Helen M.E. Duyvesteyn, Raksha Das, Donal Skelly, Thomas G. Ritter, Ali Amini, Sagida Bibi, Sandra Adele, Sile Ann Johnson, Bede Constantinides, Hermione Webster, Nigel Temperton, Paul Klenerman, Eleanor Barnes, Susanna J. Dunachie, Derrick Crook, Andrew J. Pollard, Teresa Lambe, Philip Goulder, Neil G. Paterson, Mark A. Williams, David R. Hall, OPTIC consortium, ISARIC4C consortium, Elizabeth E. Fry, Juthathip Mongkolsapaya, Jingshan Ren, David I. Stuart, Gavin R. Screaton

PII: S0092-8674(22)00710-3

DOI: https://doi.org/10.1016/j.cell.2022.06.005

Reference: CELL 12507

To appear in: *Cell*

Received Date: 6 May 2022

Revised Date: 23 May 2022

Accepted Date: 3 June 2022

Please cite this article as: Tuekprakhon, A., Huo, J., Nutalai, R., Dijokaite-Guraliuc, A., Zhou, D., Ginn, H.M., Selvaraj, M., Liu, C., Mentzer, A.J., Supasa, P., Duyvesteyn, H.M.E., Das, R., Skelly, D., Ritter, T.G., Amini, A., Bibi, S., Adele, S., Johnson, S.A., Constantinides, B., Webster, H., Temperton, N., Klenerman, P., Barnes, E., Dunachie, S.J., Crook, D., Pollard, A.J, Lambe, T., Goulder, P., Paterson, N.G., Williams, M.A., Hall, D.R., OPTIC consortium, ISARIC4C consortium, Fry, E.E., Mongkolsapaya, J., Ren, J., Stuart, D.I., Screaton, G.R, Antibody escape of SARS-CoV-2 Omicron BA.4 and BA.5 from vaccine and BA.1 serum *Cell* (2022), doi: https://doi.org/10.1016/j.cell.2022.06.005.

during the production process, errors may be discovered which could affect the content, and all legal disclaimers that apply to the journal pertain.

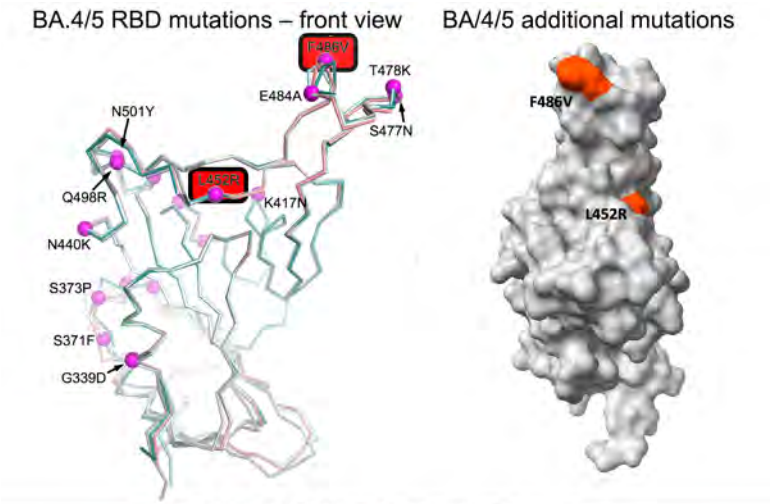

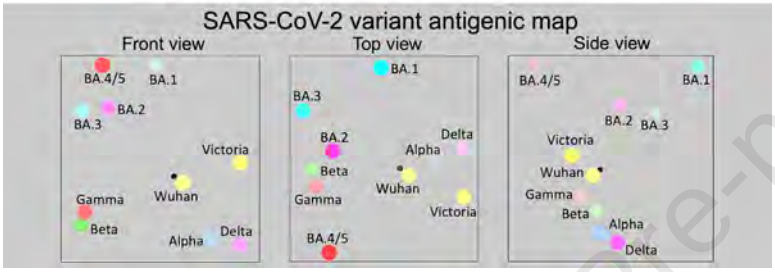

Antibody escape of SARS-CoV-2 Omicron BA.4 and BA.5 from vaccine and BA.1 serum

Aekkachai Tuekprakhon[1,#], Jiandong Huo[2,#], Rungtiwa Nutalai[1,#], Aiste Dijokaite-Guraliuc[1,#], Daming Zhou[2,3,#], Helen M. Ginn[4], Muneeswaran Selvaraj[1], Chang Liu[1,3], Alexander J. Mentzer[1,5], Piyada Supasa[1], Helen M.E. Duyvesteyn[2], Raksha Das[1], Donal Skelly[5,6,7], Thomas G. Ritter[5], Ali Amini[5,6,8], Sagida Bibi[9], Sandra Adele[5], Sile Ann Johnson[5], Bede Constantinides[10], Hermione Webster[10], Nigel Temperton[11], Paul Klenerman[5,6,8,12], Eleanor Barnes[5,6,8,12], Susanna J. Dunachie[5,6,13,14], Derrick Crook[10], Andrew J Pollard[9,12], Teresa Lambe[3,9], Philip Goulder[6,15], Neil G. Paterson[4], Mark A. Williams[4], David R. Hall[4], OPTIC consortium[&], ISARIC4C consortium[$], Elizabeth E. Fry[2*], Juthathip Mongkolsapaya[1,3,*], Jingshan Ren[2,*], David I. Stuart[2,3,4,*,^], Gavin R Screaton[1,3,*]

1. Wellcome Centre for Human Genetics, Nuffield Department of Medicine, University of Oxford, Oxford, UK
2. Division of Structural Biology, Nuffield Department of Medicine, University of Oxford, The Wellcome Centre for Human Genetics, Oxford, UK
3. Chinese Academy of Medical Science (CAMS) Oxford Institute (COI), University of Oxford, Oxford, UK
4. Diamond Light Source Ltd, Harwell Science & Innovation Campus, Didcot, UK
5. Oxford University Hospitals NHS Foundation Trust, Oxford, UK
6. Peter Medawar Building for Pathogen Research, Oxford, UK
7. Nuffield Department of Clinical Neurosciences, University of Oxford, Oxford, UK
8. Translational Gastroenterology Unit, University of Oxford, Oxford, UK
9. Oxford Vaccine Group, Department of Paediatrics, University of Oxford, Oxford, UK
10. Nuffield Department of Medicine, University of Oxford, Oxford, UK
11. Viral Pseudotype Unit, Medway School of Pharmacy, University of Kent and Greenwich Chatham Maritime, Kent ME4 4TB, UK
12. NIHR Oxford Biomedical Research Centre, Oxford, UK
13. Centre For Tropical Medicine and Global Health, Nuffield Department of Medicine, University of Oxford, Oxford, UK
14. Mahidol-Oxford Tropical Medicine Research Unit, Bangkok, Thailand, Department of Medicine, University of Oxford, Oxford, UK
15. Department of Paediatrics, University of Oxford, Oxford, UK.

# These authors contributed equally to this work.
&,$ See acknowledgements
* Corresponding authors: whgu0813@ox.ac.uk, ren@strubi.ox.ac.uk, dave@strubi.ox.ac.uk, gavin.screaton@medsci.ox.ac.uk
^ Lead contact

Summary

The Omicron lineage of SARS-CoV-2, first described in November 2021, spread rapidly to become globally dominant and has split into a number of sub-lineages. BA.1 dominated the initial wave but has been replaced by BA.2 in many countries. Recent sequencing from South Africa's Gauteng region uncovered two new sub-lineages, BA.4 and BA.5 which are taking over locally, driving a new wave. BA.4 and BA.5 contain identical spike sequences and, although closely related to BA.2, contain further mutations in the receptor binding domain of spike. Here, we study the neutralization of BA.4/5 using a range of vaccine and naturally immune serum and panels of monoclonal antibodies. BA.4/5 shows reduced neutralization by serum from triple AstraZeneca or Pfizer vaccinated individuals compared to BA.1 and BA.2. Furthermore, using serum from BA.1 vaccine breakthrough infections there are likewise, significant reductions in the neutralization of BA.4/5, raising the possibility of repeat Omicron infections.

Introduction

SARS-CoV-2 emerged in Wuhan in late 2019 to rapidly cause a global pandemic. It is now estimated to have infected over half a billion people and caused over 6 million deaths (https://covid19.who.int/). Although SARS-CoV-2 RNA polymerase possesses some proofreading ability there has been rapid evolution of the viral sequence; because of the scale of the pandemic it is estimated that all single point mutations in the large SARS-CoV-2 genome will be generated every day (Sender et al., 2021). Most mutations will be silent, deleterious or of little consequence, however a few may give the virus an advantage leading to rapid natural selection (Domingo, 2010). Many thousands of individual mutations have been described, and about a year after the outbreak started, strains began to emerge containing multiple mutations, particularly in the spike (S) gene. Several of these have been designated variants of concern

(VoC) (https://www.cdc.gov/coronavirus/2019-ncov/variants/variant-classifications.html) and have led to successive waves of infection: first Alpha (Supasa et al., 2021), then Delta (Liu et al., 2021a), then Omicron (Dejnirattisai et al., 2022) spread globally becoming the dominant variants. Alongside these, Beta (Zhou et al., 2021) and Gamma (Dejnirattisai et al., 2021b) caused large regional outbreaks in Southern Africa and South America respectively but did not dominate globally. As of 29th April, over 2.5 million cases of Omicron (BA.1 and BA.2) have been reported in the UK alone (https://www.gov.uk/government/publications/covid-19-variants-genomically-confirmed-case-numbers/variants-distribution-of-case-data-29-april-2022#omicron) and, although the disease is less severe, particularly in the vaccinated, the scale of the outbreak has still led to a large number of deaths (Nealon and Cowling, 2022).

S is the major surface glycoprotein on SARS-CoV-2 and assembles into extended transmembrane anchored trimers (Walls et al., 2020; Wrapp et al., 2020), which give virions their characteristic spiky shape. S is divided into N-terminal S1 and C-terminal S2 regions. S1 contains the N-terminal domain (NTD) and receptor binding domain (RBD). A small 25 amino acid (aa) patch at the tip of the RBD is responsible for interaction with the cellular receptor ACE2 (Lan et al., 2020). Following ACE2 binding, S1 is cleaved and detaches, whilst S2 undergoes a major conformational change to expose the fusion loop, which mediates fusion of viral and host membranes, allowing the viral RNA to enter the host cell cytoplasm and commence the replicative cycle (Walls et al., 2017).

S is the major target for neutralising antibodies, and studies by a number of groups have isolated panels of monoclonal antibodies from infected or vaccinated volunteers (Barnes et al., 2020; Dejnirattisai et al., 2021a; Yuan et al., 2020a). Potently neutralizing antibodies are largely confined to three sets of sites on S1. The first is within the NTD (Cerutti et al., 2021; Chi et al.,

2020), these antibodies do not block ACE2 interaction and their mechanism of action is still not well determined. A second region of binding is on or in close proximity to the ACE2 binding surface of the RBD; most potently neutralizing antibodies bind this region and prevent interaction of S with ACE2 on the host cell, blocking infection (Dejnirattisai et al., 2021a; Yuan et al., 2020a). Finally, some potent antibodies bind the RBD but do not block ACE2 binding, exemplified by mAb S309 which binds in the region of the N-linked glycan at position 343 (Pinto et al., 2020), these antibodies may function to destabilize the S-trimer (Huo et al., 2020b; Yuan et al., 2020b; Zhou et al., 2020).

Although mutations in the VoC are spread throughout S, there are particular hotspots in the NTD and RBD, exactly where potent neutralizing antibodies bind and they are likely being driven by escape from the antibody response following natural infection or vaccination. Mutation of the ACE2 interacting surface may also give advantage by increased ACE2 affinity for S, or possibly altering receptor tropism (Zahradnik et al., 2021). Increased ACE2 affinity has been found in VoC compared to ancestral strains (Dejnirattisai et al., 2021b; Liu et al., 2021a; Supasa et al., 2021; Zhou et al., 2021), potentially conferring a transmission advantage, but affinity is not increased in Omicron BA.1 (Dejnirattisai et al., 2022) and only marginally in BA.2 (Nutalai et al., 2022).

The initial Omicron wave was caused by the BA.1 strain which, compared to ancestral strains, contains 30 aa substitutions, 6 aa deletions and 3 aa insertions, largely clustered at the sites of interaction of potently neutralizing antibodies: the ACE2 interacting surface; around the N-343 glycan, and in the NTD (Dejnirattisai et al., 2022). These changes cause large reductions in the neutralization titres of vaccine or naturally immune serum, leading to high-levels of vaccine

115 breakthrough infections and contributing to the intensity of the Omicron wave of infection
116 (Dejnirattisai et al., 2022; McCallum et al., 2022).
117
118 A number of Omicron sub-lineages have been described. BA.2 and BA.3 were reported at
119 about the same time as BA.1 and are highly related, but contain some unique changes in S
120 (**Figure 1A**), whilst another sub-lineage BA.1.1, which contains an additional R346K mutation
121 also emerged (Nutalai et al., 2022). The BA.2 strain, which possesses a small transmission
122 advantage, has become globally dominant. BA.3, reported in relatively few sequences
123 compared to BA.1 and BA.2, appears to be a mosaic of BA.1 and BA.2 changes (with 3
124 differences in the RBD compared to BA.1 and 3 differences compared to BA.2). Cases of BA.2
125 infection following BA.1, are not thought to be common, due to good levels of cross-
126 neutralizing antibody following vaccination (Nutalai et al, 2022,
127 https://www.who.int/news/item/22-02-2022-statement-on-omicron-sublineage-ba.2).
128
129 In early April 2022 two new Omicron lineages were reported from Gauteng in South Africa
130 and designated BA.4 and BA.5
131 (https://assets.publishing.service.gov.uk/government/uploads/system/uploads/attachment_dat
132 a/file/1067672/Technical-Briefing-40-8April2022.pdf). These have become dominant in
133 Gauteng and look to be fuelling a new wave of infection in South Africa, with some
134 international spread. BA.4 and BA.5 (from here on referred to as BA.4/5), have identical S
135 sequences, and appear to have evolved from BA.2. They contain additional mutations in the
136 RBD; in particular, the reversion mutation R493Q (Q493 is found in ancestral strains), together
137 with mutations L452R and F486V (**Figure 1A**).
138

Here we report the antigenic characterisation of BA.4/5 compared to the other Omicron sub-lineages (for completeness we also report data on BA.3, although this is of less concern). We find neutralization of BA.4/5 by triple dosed vaccine serum is reduced compared to BA.1 and BA.2. We also see reductions in titres against BA.4/5 compared to BA.1 and BA.2 in sera from cases who had suffered vaccine breakthrough BA.1 infections. Neutralization of the Omicron lineage by a panel of recently derived potent Omicron specific mAbs, raised following vaccine breakthrough BA.1 infection (Nutalai et al., 2022) is reduced: 10/28 are completely knocked out against BA.4/5, while several others suffer large reductions in activity compared to the other Omicron lineages. We corroborate the neutralisation results with biophysical analysis of binding, and provide structure-function explanations for mAb failure against BA.4/5 with the changes at residues 452 and 486, both of which cause serious impact. Finally, we measure the affinity of the BA.4/5 RBD for ACE2 and find that it is higher than earlier Omicron strains BA.1 and BA.2.

Results

The Omicron lineages BA.4/5

BA.4 and BA.5 S sequences are identical, and closely related to BA.2 (sequence diversity in Omicron S is shown in **Figure 1A)**. Compared to BA.2, BA.4/5 has residues 69 and 70 deleted, and contains 2 additional substitutions in the RBD: L452R and F486V, finally BA.4/5 lacks the Q493R change seen in BA.1 and BA.2, reverting to Q493 as in the Victoria/Wuhan strain.

The 2 additional mutations in the RBD are of most concern in terms of antibody escape: L452R is a chemically radical change and is one of the pair of changes in Delta RBD (the other, T478K, is already found in the Omicron lineage) L452R is also found in Epsilon and the recently reported Omicron BA.2.11 (https://www.who.int/activities/tracking-SARS-CoV-2-

variants). Mutation F486L was found in sequences of SARS-CoV-2 isolated from Mink early in the pandemic, F486 is also a site of escape mutations to several mAbs (Gobeil et al., 2021) and F486I was noted during SARS-CoV-2 evolution in an immunocompromised individual (Clark et al., 2021). The change F486V in BA.4/5 also causes a reduction in the bulk of the hydrophobic side-chain as in F486L, but is more significant. Both residues 452 and 486 lie close to the edge of the ACE2 interaction surface (**Figure 1B**) and, together with the reversion to ancestral sequence Q493 which lies within the ACE2 footprint, have the potential to modulate ACE2 affinity and the neutralizing capacity of vaccine or naturally acquired serum. The L452R and F486V mutations are likely to cause more antibody escape, while the reversion at 493 may reduce the escape from responses to earlier viruses.

To verify structural inferences the crystal structure of BA.4/5 RBD was determined at 1.9 Å as a ternary complex with a neutralising Fab and nanobody (**Table S1, Figure S1**). This confirmed that the structure of the BA.4/5 RBD is very similar to that of other variants, although the residue 371-375 region, which is a hotspot of Omicron specific mutations is unusually well ordered and the tip of the arginine side chain of L452R is found in two conformations (**Figure S1**).

Neutralization of BA.4/5 by vaccine serum

We constructed a panel of pseudotyped lentiviruses (Di Genova et al., 2020) expressing the S gene from the Omicron sub-lineages BA.1, BA.1.1, BA.2, BA.3 and BA.4/5 together with early pandemic Wuhan related strain, Victoria, used as control. Neutralization assays were performed using serum obtained 28 days following a third dose of the Oxford-AstraZeneca vaccine AZD1222 (n = 41) (Flaxman et al., 2021) or of Pfizer-BioNtech vaccine BNT162b2 (n = 19) (Cele et al., 2021a) (**Figure 2 A, B**). For AZD1222, neutralization titres for BA.4/5

were reduced 2.1-fold compared to BA.1 ($p<0.0001$) and 1.8-fold compared to BA.2 ($p<0.0001$). For BNT162b2, neutralization titres were reduced 3.1-fold ($p<0.0001$) and 3.1-fold ($p<0.0001$) compared to BA.1 and BA.2 respectively. These reductions in titre may reduce the effectiveness of vaccine at preventing infection, particularly at longer time points as antibody titres naturally wane, although it would be expected that protection would remain against severe disease.

Neutralization of BA.4/5 by serum from breakthrough BA.1 infection

Early in the Omicron outbreak when BA.1 predominated we recruited vaccinated volunteers who had suffered PCR confirmed SARS-CoV2 infection, most were sequence confirmed BA.1 infection or contacts of BA.1 confirmed cases, all of infections were mild. Early samples (n=12, 9F, 3M, median age 26, median time since vaccine 141 days) were taken ≤17 days from symptom onset (median 12 days), later samples (n=14, 7F, 7M, median age 23, median time since vaccine 111 days) were taken ≥ 28 days following symptom onset (median 45 days). All cases had been vaccinated and all but 2 had received 2 doses, 3 of the late convalescent cases received a third dose of vaccine following Omicron infection. Pseudoviral neutralization assays were performed against the panel of pseudoviruses described above (**Figure 2C, D**).

As we have previously described, BA.1 infection following vaccination leads to a broad neutralizing response, with high titres to all the VoC, which is boosted at later time points (Nutalai et al., 2022). Neutralization titres against BA.4/5 were significantly less than BA.1 and BA.2; at the early time point, BA.4/5 titres were reduced 1.9-fold ($p=0.0005$) and 1.5-fold ($p=0.0015$) compared to BA.1 and BA.2 respectively. At the later point BA.4/5 titres were reduced 3.4-fold ($p=0.0001$) and 2-fold ($p=0.0017$) compared to BA.1 and BA.2 respectively.

Thus, BA.4/5 shows a degree of immune escape from the vaccine/BA.1 response when compared with BA.1 and BA.2. These samples were all taken reasonably close to the time of infection meaning that further waning in the intervening months may render individuals susceptible to reinfection with BA.4/5.

Escape from monoclonal antibodies by BA.4/5

We have recently reported a panel of potent human mAb generated from cases of Omicron breakthrough infection (Nutalai et al., 2022). For the 28 most potent mAbs (BA.1 IC50 titres <100 ng/ml) we used pseudoviral assays to compare BA.4/5 neutralization with neutralization of BA.1, BA.1.1, BA.2 and BA.3 (**Figures 3, S2**). Neutralization of BA.4/5 was completely knocked out for 10/28 mAbs. Four further mAbs (Omi-09, 12, 29 and 35) showed >5-fold reduction in the neutralization titre of BA.4/5 compared to BA.2. All of these antibodies interact with the RBD, with the exception of Omi-41, which binds the NTD and specifically neutralizes BA.1, BA.1.1 and BA.3 but not BA.2 or BA.4/5 (for unknown reasons Omi-41 can neutralize WT Victoria virus but not Victoria pseudovirus)(Nutalai et al., 2022).

Sensitivity to L452R: We have previously reported that Omi-24, 30, 31, 34 and 41 show complete knock out of neutralizing activity against Delta, with Omi-06 showing severe knock-down of activity (Nutalai et al., 2022). Since BA.1 and BA.2 harbour only one (T478K) of the 2 Delta RBD mutations, whilst BA.4/5 also harbour L452R, we would expect all five of these L452 directed mAbs to be knocked out on BA.4/5. This is indeed observed (**Figures 3, S2**). Omi-41 also fails to neutralize, which is attributed to the differences in mutations in the NTD (**Figure 1A**).

To confirm that the neutralization effects observed are directly attributable to alterations in RBD interactions we also performed binding analyses of selected antibodies to BA.4/5 and BA.2 RBDs by surface plasmon resonance (SPR) (**Figures 4, S3**). Omi-31 was chosen as representative of the set of L452R sensitive antibodies, and as expected the binding is severely affected (**Figure 4A**). Since we have detailed information on the interaction of several Omicron responsive antibodies with the RBD, including Omi-31, we modelled the BA.4/5 RBD mutations in the context of known structures for Omicron Fabs complexed with BA.1 or Delta RBDs (Dejnirattisai et al., 2022; Nutalai et al., 2022), (**Figure 5)**. The Omi-31 complex is shown in **Figure 5A** and shows L452 tucked neatly into a hydrophobic pocket, which is unable to accommodate the larger positively charged arginine in BA.4/5 and Delta without major conformational changes.

L452R enhancement of binding: Omi-32 shows 77-fold enhanced neutralization of BA.4/5 compared to BA.2. Kinetic analysis of Fab binding to the RBDs suggests that this is mainly achieved by a 5-fold increase in the on-rate of binding (**Figure 4B, C**). This could be explained by the arginine at 452 making a salt bridge to residue 99 of the heavy chain (HC) CDR3 (**Figure 5B**). It is possible that electrostatic changes enhance on-rate by electrostatic steering of the incoming antibody.

Sensitivity to F486V: Extending the logic used to understand Delta sensitivity, the remaining antibodies affected by BA.4/5 > BA.2, but which retain activity against Delta, namely Omi-02, 09, 12, 23, 25, 26, 29, are likely sensitive to the F486V change. The binding sensitivity was confirmed by SPR analysis of Omi-12, a VH1-58 family member which, like AZD 8895 (below), binds over F486 (Nutalai et al., 2022) (**Figure 4D, E**) and showed an almost 1,000-fold reduction in affinity to BA.4/5.

Another example of the structural basis of sensitivity to F486V is provided by Omi-25 which shows reduced binding and no neutralizing activity against BA.4/5 (**Figures 3, S3J**); the Omi-25 complex shows that the phenylalanine side chain acts as a binding hot-spot, nestled in a hydrophobic cavity making favorable ring-stacking interactions with Y106 of the HC CDR3 (**Figure 5C**).

Activity of commercial antibodies against BA.4/5

We tested a panel of antibodies that have been developed for therapeutic/prophylactic use against BA.4/5 (**Figures 3, S4**). Many of these antibodies have already suffered severe reductions or knock out of activity against BA.1, BA.1.1 or BA.2. For AstraZeneca AZD1061, activity to BA.4/5 was similar to BA.2 (< 2-fold reduction), whilst for AZD8895 residual activity against BA.2 was knocked out. The activity of the combination of both antibodies in AZD7442 (Dong et al., 2021) was reduced 8.1-fold compared with BA.2. The residual activity of REG10987 (Weinreich et al., 2021) against BA.2 was further reduced on BA.4/5, likewise residual BA.1 neutralizing activity was knocked out for ADG20 (Yuan et al., 2022) on BA.4/5. For S309 (VIR-7831/7832) (Sun and Ho, 2020), activity against BA.4/5 was 1.6 fold reduced compared to BA.2.

These effects can be rationalized by reference to the way the antibodies interact with the RBD, for instance in the case of AZD8895 (an IGHV1-58 genotype mAb, **Figure 5D**), F486 forms a hydrophobic interaction hotspot which will be abrogated by the mutation to a much smaller valine sidechain. Antibody residues involved in the interactions with F486 are highly conserved among this genotype of mAbs, including Omi-12, 253 and Beta-47 (Nutalai et al.,

2022; Dejnirattisai et al., 2021a; Liu et al., 2021b), explaining the severe effect of the F486V mutation on neutralization of these mAbs (**Figures 3, S5**).

Systematic themes in mAb interactions

Both Omi-3 (a representative of the IGVH3-53 gene family) and AZD8895 (IGVH1-58) make contacts with F486. Whilst the F486V mutation has little effect on Omi-3 (**Figures 3, 4F,G, 5E**), it seriously reduces the neutralization of AZD8895 and other IGVH1-58 mAbs e.g. Omi-12 (**Figures 3, 4D,E, 5D**). It is notable that whereas the numerous Omi series antibodies belonging to the closely related IGVH3-53 and IGVH3-66 gene families (9/28 in total **Figure S2**) are almost entirely resilient to the BA.4/5 changes, the large majority of antibodies from these gene families elicited against earlier variants are knocked out on BA.1 and BA.2 (Nutalai et al., 2022), consistent with selection of a subset of antibodies by breakthrough Omicron infection that are insensitive to the further BA.4/5 mutations.

The effects on antibodies with broadly similar epitopes can vary dramatically, and this is equally true for antibodies which have 452 or 486 central to their binding footprint. Thus Omi-31 (IGVH1-69) and Omi-32 (IGVH3-33), both bind in front of the right shoulder with their CDR-H3 positioned close to 452, whilst the activity of Omi-31 is abolished by L452R (as detailed above), Omi-32 is markedly enhanced (**Figures 3, 5A,B, S2**). Similarly, Omi-25 and Omi-42 both belong to the IGVH3-9 gene family and their footprints are in the 486 region (**Figures 5C, F**). Omi-25 contacts F486, thus neutralization of BA.4/5 is abolished. In contrast Omi-42 does not contact either of the mutation sites and neutralization is fully retained for BA.4/5 (**Figures 3, 4H, I, 5F**).

ACE2 RBD affinity

We measured the affinity of BA.4/5 RBD for ACE2 by SPR (**Figure 6A-D**). The affinity of BA.4/5 RBD was increased compared to the ancestral virus (Wuhan), BA.1 and BA.2 (approximately 3-fold , 3-fold and 2-fold, respectively (BA.4/5/ACE2 KD = 2.4 nM) (Dejnirattisai et al., 2022; Nutalai et al., 2022), which is mainly attributed to an increase in binding half-life, modelling of the ACE2/RBD complex suggests that the bulk of this effect comes from the electrostatic complemantary between ACE2 and the RBD contributed by the L452R mutation (**Figure 6E-G**).

Antigenic cartography

The neutralization data above has been used to place BA.3 and BA.4/5 on an antigenic map. We repeated the method used for analysis of the Delta and Omicron variants (Liu et al., 2021a), where individual viruses were independently modelled allowing for serum specific scaling of the responses (Methods). The measured and modelled responses are shown in **Figure 7A** (with 1551 observations and 340 parameters the residual error is 23 %). The results are best visualized in three dimensions, see **Video S1**, but 2D projections are shown in **Figure 7B**. This shows, as expected, that the Omicron sub-lineages are clustered together but well separated from early pandemic virus and earlier VoC. Amongst the Omicron cluster BA.4/5 is the most distant from the pre-Omicron viruses, at a similar distance from BA.2 as BA.2 lies from BA.1.

Discussion

Following its emergence in November 2019, a succession of SARS-CoV-2 viral variants have appeared with increased fitness, which have rapidly outcompeted the preceding strain and spread globally, the most recent, Omicron appearing in late 2021.

Despite the availability of vaccines, the pandemic has not been brought under control and through Omicron, infections are as high as ever. Although vaccines are effective at preventing severe disease, they are less effective at preventing transmission, particularly of the Omicron sub-lineages. The very high level of viral replication globally drives the accrual of mutations in the viral genome and we are now seeing the assembly of dozens of individual changes in single viruses. Virus recombination, which was predicted, is now being detected, allowing shuffling of complex genomes, such as XD (Delta/BA.1) and XE (BA.1/BA.2), which in the latter case may be more transmissible (https://assets.publishing.service.gov.uk/government/uploads/system/uploads/attachment_data/file/1063424/Tech-Briefing-39-25March2022_FINAL.pdf).

How such large sequence jumps, such as that to the Omicron lineage occur is not known. It has been suggested that these may be occurring in immunocompromised or HIV infected cases, where chronic infections have been documented to last for many months or in some cases over a year. Selection of antibody escape mutations has been documented in such individuals (Cele et al., 2021b; Karim et al., 2021; Kemp et al., 2021) and successive rounds of replication, recombination and perhaps reinfection may be responsible for the selection of the constellation of S mutations found in the Omicron lineage.

BA.4/5, the most recently reported Omicron sub-lineages, seem to be taking hold in South Africa and may spread globally to replace BA.2. Although highly related to BA.2, BA.4/5 contain the 69-70 deletion in the NTD which was also found in Alpha, BA.1 and BA.3, together with additional mutations in the RBD (L452R and F486V). Thus, BA.4/5 has assembled mutations at all of the previously described positions in the VoC Alpha (N501Y), Beta (K417N,

E484K, N501Y), Gamma (K417T, E484K, N501Y) and Delta (T478K, L452), the only difference being E484A in BA.4/5 rather than E484K found in Beta and Gamma.

Here, we report greater escape from neutralization of BA.4/5 compared to BA.1 and BA.2. Serum from triple vaccinated donors has ~2-3-fold reduction in neutralization titres compared to the neutralization of BA.1 and BA.2. Additionally, serum from breakthrough BA.1 infections in vaccinees shows ~2-3-fold reduction in neutralization titres to BA.4/5 compared to BA.1 and BA.2. These reductions are in good agreement with reductions of BA.4 and BA.5 neutralization titres reported following BA.1 vaccine breakthrough infections (Khan et al., 2022). These data suggest that a further wave of Omicron infection, driven by BA.4/5 is likely, partly due to breakthrough of vaccine and naturally acquired immunity, although there is no evidence yet of increased disease severity.

Using a panel of potent mAbs generated from vaccinated cases infected with BA.1 we show the importance of the two new RBD mutations in BA.4/5. The activity of many mAbs is either knocked out or severely impaired against BA.4/5 compared to BA.2. From the neutralization data on BA.4/5, compared to that on Delta, we have been able to impute the contribution of L452R and F486V, and by combining with SPR data, as well as previous mapping by BLI competition matrices and detailed structural data (Nutalai et al., 2022) we are able to understand the basis of these effects on neutralisation and show that the L452R and F486V mutations both make major contributions to BA.4/5 escape.

It is clear that the Omicron lineage, and particularly BA.4/5, has escaped or reduced the activity of mAbs developed for clinical use, with most mAb showing complete knock out of activity. AZD7442 still shows activity against BA.4/5 (65 ng/ml), but 65-fold less than activity against

Victoria, and S309 activity against BA.4/5 is 8-fold reduced compared to Wuhan with IC50 titres >1000 ng/ml. The reduction of neutralizing activity of S309 reported here using pseudoviruses is less than that for wild type viruses and may be due to differences in the assay format, for instance the IC50 for BA.2 using pseudovirus is 638 ng/ml whilst we reported 5035 ng/ml using a wild type virus (Nutalai et al., 2022).

New monoclonals and combinations may be needed to plug the gap in activity, to protect the extremely vulnerable and those unable to mount adequate vaccine responses. There is also a question about vaccines, all current vaccines use spike derived from the original virus isolated from Wuhan. Vaccines have been remarkably effective at reducing severe disease and a triple dosing schedule has provided, at least in the short term, protection against Omicron. However, prevention of transmission may become less effective as viruses evolve antigenically further from ancestral strains. Some argue for next-generation vaccines tailored to antigenically distant strains such as Omicron to give better protection, probably used in combination with boosters containing ancestral strains. Whilst vaccination is unlikely to eliminate transmission, the combination of vaccines with boosting by natural infection will probably continue to protect the majority from severe disease.

Finally, it is impossible to say where SARS-CoV-2 evolution will go next, but it is certain the virus will continue to drift antigenically. This may be a continuation along the Omicron lineage, or we may see a large jump to a completely new lineage, like the one from Delta to Omicron. The observation that of the 30 aa substitutions in BA.1, all but one was achieved by a single base change in the codon, suggests there remains plenty of antigenic space for SARS-CoV-2 to explore and the capacity for recombination, which has so far not been observed to have breakpoints within the major antigenic sites, could generate more radical antigenic shift.

Limitations of the Study

One of the limitations of this study is that serum was obtained at early time points following vaccination or breakthrough infection, titres are likely to wane thereafter. In addition, the true *in vivo* protection induced by vaccination may be underestimated using *in vitro* neutralization assays where complement, antibody dependent cell mediated cytotoxicity and T cell responses are not operative. It would also be interesting to look at BA.4/5 neutralization using serum from unvaccinated individuals who had suffered primary BA.1 infection where the degree of escape of BA.4/5 may be greater than that seen with the vaccine breakthrough BA.1 serum reported here.

Acknowledgements

This work was supported by the Chinese Academy of Medical Sciences (CAMS) Innovation Fund for Medical Science (CIFMS), China (grant number: 2018-I2M-2-002) to D.I.S. and G.R.S. We are also grateful for support from Schmidt Futures, the Red Avenue Foundation and the Oak Foundation. G.R.S. was supported by Wellcome. H.M.E.D., and J.Ren are supported by Wellcome (101122/Z/13/Z), D.I.S. and E.E.F. by the UKRI MRC (MR/N00065X/1). D.I.S. and G.R.S. are Jenner Investigators. This is a contribution from the UK Instruct-ERIC Centre. AJM is an NIHR-supported Academic Clinical Lecturer. The convalescent sampling was supported by the Medical Research Council (grant MC_PC_19059, awarded to the ISARIC-4C consortium, with a full contributor list available at https://isaric4c.net/about/authors/) and the National Institutes for Health and Oxford Biomedical Research Centre and an Oxfordshire Health Services Research Committee grant to AJM. OPTIC Consortium: Christopher Conlon, Alexandra Deeks, John Frater, Lisa Frending, Siobhan Gardiner, Anni Jämsén, Katie Jeffery, Tom Malone, Eloise Phillips, Lucy Rothwell, Lizzie Stafford. The Wellcome Centre for

435 Human Genetics is supported by the Wellcome Trust (grant 090532/Z/09/Z). The
436 computational aspects of this research were supported by the Wellcome Trust Core Award
437 Grant Number 203141/Z/16/Z and the NIHR Oxford BRC.
438
439 The Oxford Vaccine work was supported by UK Research and Innovation, Coalition for
440 Epidemic Preparedness Innovations, National Institute for Health Research (NIHR), NIHR
441 Oxford Biomedical Research Centre, Thames Valley and South Midland's NIHR Clinical
442 Research Network. We thank the Oxford Protective T-cell Immunology for COVID-19
443 (OPTIC) Clinical team for participant sample collection and the Oxford Immunology Network
444 Covid-19 Response T cell Consortium for laboratory support. We acknowledge the rapid
445 sharing of Victoria, B.1.1.7 and B.1.351 which was isolated by scientists within the National
446 Infection Service at PHE Porton Down, and the B.1.617.2 virus was kindly provided Wendy
447 Barclay and Thushan De Silva. We thank The Secretariat of National Surveillance, Ministry of
448 Health Brazil for assistance in obtaining P.1 samples. We acknowledge Diamond Light Source
449 for time on Beamline I03 under Proposal lb27009 for COVID-19 Rapid Access. This work was
450 supported by the UK Department of Health and Social Care as part of the PITCH (Protective
451 Immunity from T cells to Covid-19 in Health workers) Consortium, the UK Coronavirus
452 Immunology Consortium (UK-CIC) and the Huo Family Foundation. EB and PK are NIHR
453 Senior Investigators and PK is funded by WT109965MA and NIH (U19 I082360). SJD is
454 funded by an NIHR Global Research Professorship (NIHR300791). DS is an NIHR Academic
455 Clinical Fellow. The views expressed in this article are those of the authors and not necessarily
456 those of the National Health Service (NHS), the Department of Health and Social Care (DHSC),
457 the National Institutes for Health Research (NIHR), the Medical Research Council (MRC) or
458 Public Health, England.
459

Author Information

These authors contributed equally: A.T., J.H., R.N., D.Z.

Contributions

J.H. performed interaction affinity analyses. D.Z. performed antibody competition analyses. D.Z., J.H., J.R., D.R.H., M.A.W. and N.G.P. prepared the crystals and enabled and performed X-ray data collection. J.R., E.E.F. and D.I.S. analyzed the structural results. G.R.S., J.H., J.M., P.S., D.Z., R.N., A.T., A.D-G., M.S., R.D. and C.L. prepared the RBDs, ACE2, and antibodies, and A.T., R.N., A.D-G and M.S performed neutralization assays. R.N., A.T., and A.D-G constructed and produced pseudovirus for Omicron variants. D.C., H.W., B.C., and N.T. provided materials. H.M.G. wrote mabscape and performed mapping and cluster analysis, including sequence and antigenic space analyses. A.J.M., D.S., T.G.R., A.A., S.B., S.A., S.A.J., P.K., E.B. S.J.D., A.J.P., T.L., and P.G. assisted with patient samples and vaccine trials. E.B., S.J.D., and P.K. conceived the study of vaccinated healthcare workers and oversaw the OPTIC Healthcare Worker study and sample collection/processing, G.R.S., and D.I.S. conceived the study and wrote the initial manuscript draft with other authors providing editorial comments. All authors read and approved the manuscript.

Competing Financial Interests

G.R.S. sits on the GSK Vaccines Scientific Advisory Board and is a founder member of RQ Biotechnology. Oxford University holds intellectual property related to the Oxford-Astra Zeneca vaccine and SARS-CoV-2 mAb discovered in G.R.S's laboratory. A.J.P. is Chair of UK Dept. Health and Social Care's (DHSC) Joint Committee on Vaccination & Immunisation (JCVI) but does not participate in the JCVI COVID-19 committee, and is a member of the WHO's SAGE. The views expressed in this article do not necessarily represent the views of

DHSC, JCVI, or WHO. The University of Oxford has entered into a partnership with AstraZeneca on coronavirus vaccine development. T.L. is named as an inventor on a patent application covering this SARS-CoV-2 vaccine and was a consultant to Vaccitech for an unrelated project whilst the study was conducted. S.J.D. is a Scientific Advisor to the Scottish Parliament on COVID-19.

Figure legends

Figure 1 The Omicron sub-lineage compared to BA.4/5. (A) Comparison of S protein mutations of Omicron BA.1, BA.1.1, BA.2, BA.3 and BA.4/5 with NTD and RBD boundaries indicated. (B) Position of RBD mutations (grey surface with the ACE2 footprint in dark green). Mutations common to all Omicron lineages are shown in white (Q493R which is reverted in BA.4/5 is shown with a cross), those common to BA.1 and BA.1.1 in cyan, those unique to BA.1.1 in blue and those unique to BA.2 in magenta. Residue 371 (yellow) is mutated in all Omicron viruses but differs between BA.1 and BA.2. The N343 glycan is shown as sticks with a transparent surface.

Figure 2 Pseudoviral neutralization assays of BA.4/5 by vaccine and BA.1 immune serum. IC50 values for the indicated viruses using serum obtained from vaccinees 28 days following their third dose of vaccine (A) AstraZeneca AZD AZD1222 (n=41), (B) 4 weeks after the third dose of Pfizer BNT162b2 (n=19). Serum from volunteers suffering breakthrough BA.1 infection volunteer taken (C) early ≤17 days from symptom onset (median 12 days) n=12 (D) late ≥ 28 days from symptom onset (median 45 days) n=14. Comparison is made with neutralization titres to Victoria an early pandemic strain, BA.1, BA.1.1, BA.2 and BA.3.

509 Geometric mean titres are shown above each column. The Wilcoxon matched-pairs signed rank
510 test was used for the analysis and two-tailed P values were calculated.
511
512 **Figure 3 IC50 values for Omicron and commercial mAbs**. See also Figures S2, S3, S4 and
513 S5
514
515 **Figure 4 Surface plasmon resonance (SPR) analysis of interaction between BA.2 or**
516 **BA.4/5 RBD and selected mAbs.** (A) Binding of BA.4/5 RBD is severely reduced compared
517 to that of BA.2, so that the binding could not be accurately determined, as shown by a single-
518 injection of 200 nM RBD over sample flow cells containing IgG Omi-31. (B-C; E-I)
519 Sensorgrams (Red: original binding curve; black: fitted curve) showing the interactions
520 between BA.2 or BA.4/5 RBD and selected mAbs, with kinetics data shown. (D)
521 Determination of the affinity of BA.4/5 RBD to Omi-12 using a 1:1 binding equilibrium
522 analysis. See also Figures 3, S3.
523
524 **Figure 5 Interactions between mAb and BA.4/5 mutation sites**. Overall structure (left panel)
525 and interactions (≤ 4 Å) with BA.4/5 mutation sites (right panel) for (A) BA.1-RBD/Omi-31
526 (PDB 7ZFB), (B) BA.1-RBD/Omi-32 (PDB 7ZFE), (C) BA.1-RBD/Omi-25 (PDB 7ZFD), (D)
527 Wuhan-RBD/AZD8895 (PDB 7L7D) and (E) BA.1-RBD/Omi-3 (PDB 7ZF3) complexes, (F)
528 BA.1-RBD/Omi-42 (PDB7ZR7). In the left panels RBD is shown as surface representation,
529 with BA.4/5 mutation sites highlighted in magenta and the additional two mutation sites of
530 BA.4/5 at 452 and 486 in cyan, and Fab LC as blue and HC as red ribbons. In the right
531 panel, side chains of RBD, Fab HC and LC are drawn as grey, red and blue sticks, respectively.
532 In (B) the L452R mutation (cyan sticks) is modelled to show a salt bridge to D99 of CDR-H3

533 may be formed (yellow broken sticks). Panel (F) shows that the Fab of Omi-42 does not contact
534 either of the two BA.4/5 mutation sites. See also Figure S1.
535
536 **Figure 6 ACE2 RBD affinity.** (A)-(D) SPR sensorgrams showing ACE2 binding of BA.4/5
537 RBD (A) in comparison to binding to ancestral (Wuhan) (B), BA.1 (C) and BA.2 RBD (D).
538 The data for Wuhan, BA.1 and BA.2 have been reported previously in (Nutalai et al., 2022).
539 (E)-(G) Electrostatic surfaces, (E) from left to right, early pandemic, Delta and BA.1 RBD
540 respectively, (F) open book view of BA.2 RBD and ACE2 of the BA.2 RBD/ACE2 complex
541 (PDB 7ZF7), and (G) BA.4/5 RBD (modelled based on the structure of BA.2 RBD). The
542 lozenges on ACE2 and RBD show the interaction areas.
543
544 **Figure 7 Antigenic mapping.** (A) Neutralization data and model (log titre values) used to
545 calculate antigenic maps in (B)**.** Columns represent sera collected from inoculated volunteers
546 or infected patients. Rows are challenge strains: Victoria, Alpha, Delta, Beta, Gamma, BA.1,
547 BA1.1, BA.2, BA.3 and BA.4/5 in order. Values are colored according to their deviation from
548 the reference value; the reference value is calculated on a serum-type basis as the average of
549 neutralization titres from the row which gives this the highest value. (B) Orthogonal views of
550 the antigenic map showing BA.4/5 in the context of the positions of previous VoC and BA.1,
551 BA.1.1, BA.1 and BA.2, calculated from pseudovirus neutralisation data. Distance between
552 two positions is proportional to the reduction in neutralisation titre when one of the
553 corresponding strains is challenged with serum derived by infection by the other. No scale is
554 provided since the figures are projections of a three-dimensional distribution, however the
555 variation can be calibrated by comparison with (i) BA.1 to BA.2 which is 2.93x reduced and
556 (ii) BA.2 to BA.4/5 which is 3.03x reduced.
557

Figure S1. Overall Structure of BA.4 RBD/Beta-27 complex. (A) Comparison of BA.4 RBD/Beta-27 (the bound nanobody C1 is omitted for clarity) with Beta RBD/Beta-27 (PDB, 7PS1) by overlapping the RBDs. The RBD is shown as grey surface with mutation sites highlighted in magenta, The heavy chain and light chain are drawn as red and blue ribbons, respectively, for the BA.4 RBD/Beta-27 complex, Beta-27 in the Beta RBD complex coloured in pale cyan. The overall binding modes of the Fab in the two complexes are very similar although there are some differences in the side chain orientations at the interface, such as R403, N417 and Q493 of the RBD. The light chain CDR3 becomes flexible in the BA.4 complex. (B) Electron density maps. Residues 371-375 that carry the S371L/F, S373P and S375F mutations are flexible in the BA.1 and BA.2 RBD/Fab complexes (PDB, 7ZF3, 7ZF8), but are well ordered in this high BA.4/5 resolution structure (top panel). L452R has double conformation (middle panel) and F486V has well defined density (bottom panel). (C) Comparison of BA.4 RBD (grey) with those of BA.1 (teal), BA.2 (cyan) and Beta (salmon). Mutation sites in BA.4 are shown as magenta spheres. Related to Table S1 and Methods.

Figure S2. Pseudoviral neutralization assays against Omicron monoclonal antibodies. Neutralization curves for a panel of 28 monoclonal antibodies made from samples taken from vaccinees infected with BA.1. Titration curves for BA.4/5 are compared with Victoria, BA.1, BA.1.1, BA.2 and BA.3, mAbs we propose to be affected by the L452R and F486V mutations are indicated as are those belonging to the IGVH3-53/66 gene families. Related to Figure 3 where IC50 titres are shown.

Figure S3. Surface plasmon resonance (SPR) analysis of interaction between BA.2 or BA.4/5 RBD and selected mAbs. (A-F) Sensorgrams (Red: original binding curve; black: fitted curve) showing the interactions between BA.2 or BA.4/5 RBD and selected mAbs, with

kinetics data shown. (G-K) Binding of BA.4/5 RBD is severely reduced compared to that of BA.2, so that the binding could not be accurately determined, as shown by a single-injection of 200 nM RBD over sample flow cells containing the mAb indicated. Related to Figure 3.

Figure S4. Pseudoviral neutralization assays against commercial monoclonal antibodies. Pseudoviral neutralization assays with mAbs developed for human use. Related to Figure 3 where IC50 titres are shown.

Figure S5. Neutralization curves for VH1-58 mAb. Pseudoviral neutralization curves for early pandemic mAb 253 (Dejnirattisai et al., 2021a) and Beta-47 (Liu et al., 2021b) against Victoria and the panel of Omicron lineage constructs. Related to Figure 3.

STAR Methods

RESOURCE AVAILABILITY

Lead Contact

Resources, reagents and further information requirement should be forwarded to and will be responded by the Lead Contact, David I Stuart (dave@strubi.ox.ac.uk).

Materials Availability

Reagents generated in this study are available from the Lead Contact with a completed Materials Transfer Agreement.

Data and Code Availability

The coordinates and structure factors available from the PDB with accession code 7ZXU. Mabscape is available from https://github.com/helenginn/mabscape, https://snapcraft.io/mabscape. The data that support the findings of this study are available from the corresponding authors on request.

EXPERIMENTAL MODEL AND SUBJECT DETAILS

Bacterial Strains and Cell Culture

Vero (ATCC CCL-81) and VeroE6/TMPRSS2 cells were cultured at 37 °C in Dulbecco's Modified Eagle medium (DMEM) high glucose (Sigma-Aldrich) supplemented with 10% fetal bovine serum (FBS), 2 mM GlutaMAX (Gibco, 35050061) and 100 U/ml of penicillin–streptomycin. Human mAbs were expressed in HEK293T cells cultured in UltraDOMA PF Protein-free Medium (Cat# 12-727F, LONZA) at 37 °C with 5% CO_2. HEK293T (ATCC CRL-11268) cells were cultured in DMEM high glucose (Sigma-Aldrich) supplemented with 10% FBS, 1% 100X Mem Neaa (Gibco) and 1% 100X L-Glutamine (Gibco) at 37 °C with 5% CO_2. To express RBD, RBD variants and ACE2, HEK293T cells were cultured in DMEM high glucose (Sigma) supplemented with 2% FBS, 1% 100X Mem Neaa and 1% 100X L-Glutamine at 37 °C for transfection. Omicron RBD and human mAbs were also expressed in HEK293T (ATCC CRL-11268) cells cultured in FreeStyle 293 Expression Medium (ThermoFisher, 12338018) at 37 °C with 5% CO_2. *E.coli DH5α* bacteria were used for transformation and large-scale preparation of plasmids. A single colony was picked and cultured in LB broth at 37 °C at 200 rpm in a shaker overnight.

Plasma from early pandemic and Alpha cases

Participants from the first wave of SARS-CoV2 in the U.K. and those sequence confirmed with B.1.1.7 lineage in December 2020 and February 2021 were recruited through three studies: Sepsis Immunomics [Oxford REC C, reference:19/SC/0296]), ISARIC/WHO Clinical Characterisation Protocol for Severe Emerging Infections [Oxford REC C, reference 13/SC/0149] and the Gastro-intestinal illness in Oxford: COVID sub study [Sheffield REC, reference: 16/YH/0247]. Diagnosis was confirmed through reporting of symptoms consistent with COVID-19 and a test positive for SARS-CoV-2 using reverse transcriptase polymerase chain reaction (RT-PCR) from an upper respiratory tract (nose/throat) swab tested in accredited laboratories. A blood sample was taken following consent at least 14 days after symptom onset. Clinical information including severity of disease (mild, severe or critical infection according to recommendations from the World Health Organisation) and times between symptom onset and sampling and age of participant was captured for all individuals at the time of sampling. Following heat inactivation of plasma/serum samples they were aliquoted so that no more than 3 freeze thaw cycles were performed for data generation.

Sera from Beta, Gamma and Delta and BA.1 infected cases

Beta and Delta samples from UK infected cases were collected under the "Innate and adaptive immunity against SARS-CoV-2 in healthcare worker family and household members" protocol affiliated to the Gastro-intestinal illness in Oxford: COVID sub study discussed above and approved by the University of Oxford Central University Research Ethics Committee. All individuals had sequence confirmed Beta/Delta infection or PCR-confirmed symptomatic disease occurring whilst in isolation and in direct contact with Beta/Delta sequence-confirmed cases. Additional Beta infected serum (sequence confirmed) was obtained from South Africa. At the time of swab collection patients signed an informed consent to consent for the collection of data and serial blood samples. The study was approved by the Human Research Ethics

Committee of the University of the Witwatersrand (reference number 200313) and conducted in accordance with Good Clinical Practice guidelines. Gamma samples were provided by the International Reference Laboratory for Coronavirus at FIOCRUZ (WHO) as part of the national surveillance for coronavirus and had the approval of the FIOCRUZ ethical committee (CEP 4.128.241) to continuously receive and analyse samples of COVID-19 suspected cases for virological surveillance. Clinical samples were shared with Oxford University, UK under the MTA IOC FIOCRUZ 21-02.

Sera from BA.1 infected cases, study subjects

Following informed consent, individuals with omicron BA.1 were co-enrolled into the ISARIC/WHO Clinical Characterisation Protocol for Severe Emerging Infections [Oxford REC C, reference 13/SC/0149] and the "Innate and adaptive immunity against SARS-CoV-2 in healthcare worker family and household members" protocol affiliated to the Gastro-intestinal illness in Oxford: COVID sub study [Sheffield REC, reference: 16/YH/0247] further approved by the University of Oxford Central University Research Ethics Committee. Diagnosis was confirmed through reporting of symptoms consistent with COVID-19 or a positive contact of a known Omicron case, and a test positive for SARS-CoV-2 using reverse transcriptase polymerase chain reaction (RT-PCR) from an upper respiratory tract (nose/throat) swab tested in accredited laboratories and lineage sequence confirmed through national reference laboratories. A blood sample was taken following consent at least 10 days after PCR test confirmation. Clinical information including severity of disease (mild, severe or critical infection according to recommendations from the World Health Organisation) and times between symptom onset and sampling and age of participant was captured for all individuals at the time of sampling.

Sera from Pfizer vaccinees

Pfizer vaccine serum was obtained from volunteers who had received three doses of the BNT162b2 vaccine. Vaccinees were Health Care Workers, based at Oxford University Hospitals NHS Foundation Trust, not known to have prior infection with SARS-CoV-2 and were enrolled in the OPTIC Study as part of the Oxford Translational Gastrointestinal Unit GI Biobank Study 16/YH/0247 [research ethics committee (REC) at Yorkshire & The Humber – Sheffield] which has been amended for this purpose on 8 June 2020. The study was conducted according to the principles of the Declaration of Helsinki (2008) and the International Conference on Harmonization (ICH) Good Clinical Practice (GCP) guidelines. Written informed consent was obtained for all participants enrolled in the study. Participants were sampled approximately 28 days (range 25-56) after receiving a third "booster dose of BNT162B2 vaccine. The mean age of vaccinees was 37 years (range 22-66), 21 male and 35 female.

AstraZeneca-Oxford vaccine study procedures and sample processing

Full details of the randomized controlled trial of ChAdOx1 nCoV-19 (AZD1222), were previously published (PMID: 33220855/PMID: 32702298). These studies were registered at ISRCTN (15281137 and 89951424) and ClinicalTrials.gov (NCT04324606 and NCT04400838). Written informed consent was obtained from all participants, and the trial is being done in accordance with the principles of the Declaration of Helsinki and Good Clinical Practice. The studies were sponsored by the University of Oxford (Oxford, UK) and approval obtained from a national ethics committee (South Central Berkshire Research Ethics Committee, reference 20/SC/0145 and 20/SC/0179) and a regulatory agency in the United Kingdom (the Medicines and Healthcare Products Regulatory Agency). An independent DSMB reviewed all interim safety reports. A copy of the protocols was included in previous

publications (Folegatti et al., 2020). Data from vaccinated volunteers who received three vaccinations are included in this study. Blood samples were collected and serum separated approximately 28 days (range 26-34 days) following the third dose.

Method Details

Plasmid construction and pseudotyped lentiviral particles production

Pseudotyped lentivirus expressing SARS-CoV-2 S proteins from ancestral strain (Victoria, S247R) , BA.1, BA.1.1, and BA.2 were constructed as described previously (Nie et al., 2020, Liu et al., 2021b, Nutalai et al., 2022), with some modifications. A similar strategy was applied for BA.3 and BA.4/5, briefly, BA.3 mutations were constructed using the combination fragments from BA.1 and BA.2. The resulting mutations are as follows, A67V, Δ69-70, T95I, G142D, Δ143-145, Δ211/L212I, G339D, S371F, S373P, S375F, D405N, K417N, N440K, G446S, S477N, T478K, E484A, Q493R, Q498R, N501Y, Y505H, D614G, H655Y, N679K, P681H, N764K, D796Y, Q954H, and N969K. Although BA.4/5 S protein shared some amino acid mutations with BA.2 (Nutalai et al., 2022), to generate BA.4/5 we added mutations Δ69-70, L452R, F486V, and R498Q. The resulting S gene-carrying pcDNA3.1 was used for generating pseudoviral particles together with the lentiviral packaging vector and transfer vector encoding luciferase reporter. Integrity of constructs was sequence confirmed.

Pseudoviral neutralization test

The details of the pseudoviral neutralization test are as described previously (Liu et al., 2021b) with some modifications. Briefly, the neutralizing activity of potent monoclonal antibodies generated from donors who had recovered from Omicron were assayed against Victoria,

Omicron-BA.1, BA.1.1, BA.2, BA.3 and BA.4/5. Four-fold serial dilutions of each mAb were incubated with pseudoviral particles at 37˚C, 5% CO2 for 1 hr. Stable HEK293T/17 cells expressing human ACE2 were then added to the mixture at 1.5 x 10^4 cells/well. 48 hr post transduction, culture supernatants were removed and 50 µL of 1:2 Bright-GloTM Luciferase assay system (Promega, USA) in 1x PBS was added to each well. The reaction was incubated at room temperature for 5 mins and firefly luciferase activity was measured using CLARIOstar® (BMG Labtech, Ortenberg, Germany). The percentage neutralization was calculated relative to the control. Probit analysis was used to estimate the dilution that inhibited half maximum pseudotyped lentivirus infection (PVNT50).

To determine the neutralizing activity of convalescent plasma/serum samples or vaccine sera, 3-fold serial dilutions of samples were incubated with pseudoviral particles for 1 hr and the same strategy as mAb was applied.

Cloning of RBDs

To generate His-tagged constructs of BA.4/5 RBD, site-directed PCR mutagenesis was performed using the BA.2 RBD construct as the template (Nutalai et al., 2022), with the introduction of L452R, F486V and R493Q mutations. The gene fragment was amplified with pNeoRBD333Omi_F (5'-GGTTGCGTAGCTGAAACCGGTCATCACCATCACCATCACACCAATCTGTGCCCTTTCGAC-3') and pNeoRBD333_R (5'-GTGATGGTGGTGCTTGGTACCTTATTACTTCTTGCCGCACACGGTAGC-3'), and cloned into the pNeo vector (Supasa et al., 2021). To generate the BA.4/5 RBD construct containing a BAP-His tag, the gene fragment was amplified with RBD333_F (5'-GCGTAGCTGAAACCGGCACCAATCTGTGCCCTTTCGAC-3') and RBD333_BAP_R

(5'- GTCATTCAGCAAGCTCTTCTTGCCGCACACGGTAGC-3'), and cloned into the pOPINTTGneo-BAP vector (Huo et al., 2020a). Cloning was performed using the ClonExpress II One Step Cloning Kit (Vazyme). The Constructs were verified by Sanger sequencing after plasmid isolation using QIAGEN Miniprep kit (QIAGEN).

Production of RBDs

Plasmids encoding RBDs were transfected into Expi293F™ Cells (ThermoFisher) by PEI, cultured in FreeStyle™ 293 Expression Medium (ThermoFisher) at 30 °C with 8% CO_2 for 4 days. To express biotinylated RBDs, the RBD-BAP plasmid was co-transfected with pDisplay-BirA-ER (Addgene plasmid 20856; coding for an ER-localized biotin ligase), in the presence of 0.8 mM D-biotin (Sigma-Aldrich). The conditioned medium was diluted 1:2 into binding buffer (50 mM sodium phosphate, 500 mM sodium chloride, pH 8.0). RBDs were purified with a 5 mL HisTrap nickel column (GE Healthcare) through His-tag binding, followed by a Superdex 75 10/300 GL gel filtration column (GE Healthcare) in 10 mM HEPES and 150 mM sodium chloride.

Surface Plasmon Resonance

The surface plasmon resonance experiments were performed using a Biacore T200 (GE Healthcare). All assays were performed with running buffer of HBS-EP (Cytiva) at 25 °C.

To determine the binding kinetics between the RBDs and mAb Omi-32 / Omi-42, a Biotin CAPture Kit (Cytiva) was used. Biotinylated RBD was immobilised onto the sample flow cell of the sensor chip. The reference flow cell was left blank. The mAb Fab was injected over the two flow cells at a range of five concentrations prepared by serial two-fold dilutions, at a flow rate of 30 μl min^{-1} using a single-cycle kinetics programme. Running buffer was also injected

using the same programme for background subtraction. All data were fitted to a 1:1 binding model using Biacore T200 Evaluation Software 3.1.

To determine the binding kinetics between RBDs and ACE2 / other mAbs, a Protein A sensor chip (Cytiva) was used. ACE2-Fc or mAb in the IgG form was immobilised onto the sample flow cell of the sensor chip. The reference flow cell was left blank. RBD was injected over the two flow cells at a range of five concentrations prepared by serial two-fold dilutions, at a flow rate of 30 µl min^{-1} using a single-cycle kinetics programme. Running buffer was also injected using the same programme for background subtraction. All data were fitted to a 1:1 binding model using Biacore T200 Evaluation Software 3.1.

To determine the binding affinity of BA.4/5 RBD and mAb Omi-12, a Protein A sensor chip (Cytiva) was used. The Ig Omi-12 was immobilised onto the sample flow cell of the sensor chip. The reference flow cell was left blank. RBD was injected over the two flow cells at a range of seven concentrations prepared by serial twofold dilutions, at a flow rate of 30 µl min^{-1}. Running buffer was also injected using the same programme for background subtraction. All data were fitted to a 1:1 binding model using Prism9 (GraphPad).

To compare the binding profiles between BA.2 and BA.4/5 RBD for mAb Omi-06 / Omi-25 / Omi-26, a Protein A sensor chip (Cytiva) was used. mAb in the IgG form was immobilised onto the sample flow cell of the sensor chip to a similar level (~350 RU). The reference flow cell was left blank. A single injection of RBD was performed over the two flow cells at 200 nM, at a flow rate of 30 µl min^{-1}. Running buffer was also injected using the same programme for background subtraction. The sensorgrams were plotted using Prism9 (GraphPad).

To compare the binding profiles between BA.2 and BA.4/5 RBD for mAb Omi-02 / Omi-23 / Omi-31, a Biotin CAPture Kit (Cytiva) was used. Biotinylated BA.2 and BA.4/5 RBD was immobilised onto the sample flow cell of the sensor chip to a similar level (~120 RU). The reference flow cell was left blank. A single injection of mAb Fab was performed over the two flow cells at 200 nM, at a flow rate of 30 µl min^{-1}. Running buffer was also injected using the same programme for background subtraction. The sensorgrams were plotted using Prism9 (GraphPad).

IgG mAbs and Fabs production

AstraZeneca and Regeneron antibodies were provided by AstraZeneca, Vir, Lilly and Adagio antibodies were provided by Adagio. For the in-house antibodies, heavy and light chains of the indicated antibodies were transiently transfected into 293Y cells and antibody purified from supernatant on protein A as previously described (Nutalai et al., 2022). Fabs were digested from purified IgGs with papain using a Pierce Fab Preparation Kit (Thermo Fisher), following the manufacturer's protocol.

Crystallization, X-ray data collection and structure determination

Crystals of BA.4 RBD/Beta-27 complex were grown from 4% (v/v) 2-propanol, 0.1M BIS-Tris propane, pH9.0, 20% (w/v) PEG monomethyl ether 5000 using the sitting drop method and nanobody NbC1 as a crystallisation chaperon. Diffraction data were collected at 100 K at beamline I03 of Diamond Light Source, UK, using the automated queue system that allows unattended automated data collection (https://www.diamond.ac.uk/Instruments/Mx/I03/I03-Manual/Unattended-Data-Collections.html). Structures were determined by molecular replacement with PHASER(McCoy et al., 2007). VhVl and ChCl domains of Beta-27 (Liu et al., 2021a) and RBD/NbC1 complex (PDB, 7OAP) were used as search models. Model

rebuilding is done with COOT (Emsley et al., 2010) and refinement with Phenix (Liebschner et al., 2019).

Data collection and structure refinement statistics are given in **Table S1** and structural details in **Figure S1**. Structural comparisons used SHP (Stuart et al., 1979) and figures were prepared with PyMOL (The PyMOL Molecular Graphics System, Version 1.2r3pre, Schrödinger, LLC).

Antigenic mapping

Antigenic mapping of omicron was carried out through an extension of a previous algorithm (Liu et al., 2021a). In short, coronavirus variants were assigned three-dimensional coordinates whereby the distance between two points indicates the base drop in neutralization titre. Each serum was assigned a strength parameter which provided a scalar offset to the logarithm of the neutralization titre. These parameters were refined to match predicted neutralization titres to observed values by taking an average of superimposed positions from 30 separate runs. The three-dimensional positions of the variants of concern: Victoria, Alpha, Beta, Gamma, Delta and Omicron were plotted for display.

Quantification and statistical analysis

Statistical analyses are reported in the results and figure legends. Neutralization was measured on pseudovirus. The percentage reduction was calculated and IC_{50} determined using the probit program from the SPSS package. The Wilcoxon matched-pairs signed rank test was used for the analysis and two-tailed P values were calculated on geometric mean values.

Video S1. Antigenic landscape for SARS-CoV-2. Related to Figure 6B.

855 References
856
857 Aricescu AR, Lu W, Jones EY. A time- and cost-efficient system for high-level protein
858 production in mammalian cells. Acta Crystallogr D Biol Crystallogr. 2006 Oct;62(Pt 10):1243-
859 50. doi: 10.1107/S0907444906029799. Epub 2006 Sep 19. PMID: 17001101.
860
861 Barnes, C.O., Jette, C.A., Abernathy, M.E., Dam, K.A., Esswein, S.R., Gristick, H.B.,
862 Malyutin, A.G., Sharaf, N.G., Huey-Tubman, K.E., Lee, Y.E., *et al.* (2020). SARS-CoV-2
863 neutralizing antibody structures inform therapeutic strategies. Nature *588*, 682-687.
864
865 Cele, S., Jackson, L., Khoury, D.S., Khan, K., Moyo-Gwete, T., Tegally, H., San, J.E., Cromer,
866 D., Scheepers, C., Amoako, D.G., *et al.* (2021). Omicron extensively but incompletely escapes
867 Pfizer BNT162b2 neutralization. Nature *602*, 654-666.
868
869 Cele, S., Karim, F., Lustig, G., San, J.E., Hermanus, T., Tegally, H., Snyman, J., Moyo-Gwete,
870 T., Wilkinson, E., M., B., *et al.* (2022). SARS-CoV-2 prolonged infection during advanced
871 HIV disease evolves extensive immune escape. Cell Host Microbe *30*,154-162.
872
873 Cerutti, G., Guo, Y., Zhou, T., Gorman, J., Lee, M., Rapp, M., Reddem, E.R., Yu, J., Bahna,
874 F., Bimela, J., *et al.* (2021). Potent SARS-CoV-2 neutralizing antibodies directed against spike
875 N-terminal domain target a single supersite. Cell Host Microbe *29*, 819-833 e817.
876
877 Chi, X., Yan, R., Zhang, J., Zhang, G., Zhang, Y., Hao, M., Zhang, Z., Fan, P., Dong, Y., Yang,
878 Y., *et al.* (2020). A neutralizing human antibody binds to the N-terminal domain of the Spike
879 protein of SARS-CoV-2. Science *369*, 650-655.
880
881 Clark SA, Clark LE, Pan J, Coscia A, McKay LGA, Shankar S, Johnson RI, Brusic V,
882 Choudhary MC, Regan J, Li JZ, *et al.* (2021) SARS-CoV-2 evolution in an
883 immunocompromised host reveals shared neutralization escape mechanisms. Cell 184, 2605-
884 2617.e18.
885
886 Dejnirattisai, W., Huo, J., Zhou, D., Zahradnik, J., Supasa, P., Liu, C., Duyvesteyn, H.M.E.,
887 Ginn, H.M., Mentzer, A.J., Tuekprakhon, A., *et al.* (2022). SARS-CoV-2 Omicron-B.1.1.529
888 leads to widespread escape from neutralizing antibody responses. Cell *185*, 467-484 e415.
889
890 Dejnirattisai, W., Zhou, D., Ginn, H.M., Duyvesteyn, H.M.E., Supasa, P., Case, J.B., Zhao, Y.,
891 Walter, T.S., Mentzer, A.J., Liu, C., *et al.* (2021a). The antigenic anatomy of SARS-CoV-2
892 receptor binding domain. Cell *184*, 2183-2200 e2122.
893
894 Dejnirattisai, W., Zhou, D., Supasa, P., Liu, C., Mentzer, A.J., Ginn, H.M., Zhao, Y.,
895 Duyvesteyn, H.M.E., Tuekprakhon, A., Nutalai, R., *et al.* (2021b). Antibody evasion by the
896 P.1 strain of SARS-CoV-2. Cell *184*, 2939-2954 e2939.
897
898 Di Genova, C., Sampson, A., Scott, S., Cantoni, D., Mayora-Neto, M., Bentley, E., Mattiuzzo,
899 G., Wright, E., Derveni, M., Auld, B., *et al.* (2020). Production, titration, neutralisation and
900 storage of SARS-CoV-2 lentiviral pseudotypes. figshare.
901
902 Domingo, E. (2010). Mechanisms of viral emergence. Vet Res *41*, 38.
903

Dong, J., Zost, S., Greaney, A., Starr, T.N., Dingens, A.S., Chen, E.C., Chen, R., Case, B., Sutton, R., Gilchuk, P., *et al.* (2021). Genetic and structural basis for recognition of SARS-CoV-2 spike protein by a two-antibody cocktail. Nature Microbiol. *6*, 1233-1244.

Emsley, P., Lohkamp, B., Scott, W.G., and Cowtan, K. (2010). Features and development of Coot. Acta Crystallographica Section D: Biological Crystallography *66*, 486-501.

Flaxman, A., Marchevsky, N.G., Jenkin, D., Aboagye, J., Aley, P.K., Angus, B., Belij-Rammerstorfer, S., Bibi, S., Bittaye, M., Cappuccini, F., *et al.* (2021). Reactogenicity and immunogenicity after a late second dose or a third dose of ChAdOx1 nCoV-19 in the UK: a substudy of two randomised controlled trials (COV001 and COV002). Lancet *398*, 981-990.

Folegatti, P.M., Ewer, K.J., Aley, P.K., Angus, B., Becker, S., Belij-Rammerstorfer, S., Bellamy, D., Bibi, S., Bittaye, M., Clutterbuck, E.A., *et al.* (2020). Safety and immunogenicity of the ChAdOx1 nCoV-19 vaccine against SARS-CoV-2: a preliminary report of a phase 1/2, single-blind, randomised controlled trial. Lancet *396*, 467-478.

Gobeil, S.M., Janowska, K., McDowell, S., Mansouri, K., Parks, R., Stalls, V., Kopp, M.F., Manne, K., Li, D., Wiehe, K., *et al.* (2021). Effect of natural mutations of SARS-CoV-2 on spike structure, conformation, and antigenicity. Science *373*, 6555.

Huo, J., Le Bas, A., Ruza, R.R., Duyvesteyn, H.M.E., Mikolajek, H., Malinauskas, T., Tan, T.K., Rijal, P., Dumoux, M., Ward, P.N., *et al.* (2020a). Neutralizing nanobodies bind SARS-CoV-2 spike RBD and block interaction with ACE2. Nature structural & molecular biology *27*, 846-854.

Huo, J., Zhao, Y., Ren, J., Zhou, D., Duyvesteyn, H.M.E., Ginn, H.M., Carrique, L., Malinauskas, T., Ruza, R.R., Shah, P.N.M., *et al.* (2020b). Neutralization of SARS-CoV-2 by Destruction of the Prefusion Spike. Cell Host Microbe *28*, 445-454.

Khan,K., Karim, F., Ganga, Y., Bernstein, M., Jule, Z., Reedoy, K., Cele, S., Lustig, G., Amoako, D., Wolter, N. (2022). Omicron sub-lineages BA.4/BA.5 escape BA.1 infection elicited neutralizing immunity. medRxiv https://doi.org/10.1101/2022.04.29.22274477.

Karim, F., Moosa, M.Y.S., Gosnell, B.I., Cele, S., Giandhari, J., Pillay, S., Tegally, H., Wilkinson, E., San, J.E., Msomi, N., *et al.* (2021). Persistent SARS-CoV-2 infection and intra-host evolution in association with advanced HIV nfection medRxiv https://doi.org/10.1101/2021.06.03.21258228

Kemp, S.A., Collier, D.A., Datir, R.P., Ferreira, I., Gayed, S., Jahun, A., Hosmillo, M., Rees-Spear, C., Mlcochova, P., Lumb, I.U., *et al.* (2021). SARS-CoV-2 evolution during treatment of chronic infection. Nature *592*, 277-282.

Lan, J., Ge, J., Yu, J., Shan, S., Zhou, H., Fan, S., Zhang, Q., Shi, X., Wang, Q., Zhang, L., *et al.* (2020). Structure of the SARS-CoV-2 spike receptor-binding domain bound to the ACE2 receptor. Nature *581*, 215-220.

Libby RT, Cosman D, Cooney MK, Merriam JE, March CJ, Hopp TP. Human rhinovirus 3C protease: cloning and expression of an active form in Escherichia coli. Biochemistry. 1988 Aug 23;27(17):6262-8. doi: 10.1021/bi00417a010.

Liebschner, D., Afonine, P.V., Baker, M.L., Bunkoczi, G., Chen, V.B., Croll, T.I., Hintze, B., Hung, L.W., Jain, S., McCoy, A.J., *et al.* (2019). Macromolecular structure determination using X-rays, neutrons and electrons: recent developments in Phenix. Acta Crystallogr D Struct Biol *75*, 861-877.

Liu, C., Ginn, H.M., Dejnirattisai, W., Supasa, P., Wang, B., Tuekprakhon, A., Nutalai, R., Zhou, D., Mentzer, A.J., Zhao, Y., *et al.* (2021a). Reduced neutralization of SARS-CoV-2 B.1.617 by vaccine and convalescent serum. Cell *184*, 4220-4236 e4213.

Liu, C., Zhou, D., Nutalai, R., Duyvestyn, H., Tuekprakhon, A., Ginn, H., Dejnirattisai, W., Supasa, P., Mentzer, A., Wang, B., *et al.* (2021b). The Beta mAb response underscores the antigenic distance to other SARS-CoV-2 variants. Cell, Host and Microbe *30*, 53-68.

McCallum, M., Czudnochowski, N., Rosen, L.E., Zepeda, S.K., Bowen, J.E., Walls, A.C., Hauser, K., Joshi, A., Stewart, C., Dillen, J.R., *et al.* (2022). Structural basis of SARS-CoV-2 Omicron immune evasion and receptor engagement. Science, *375*, 864-868..

Nealon, J., and Cowling, B.J. (2022). Omicron severity: milder but not mild. Lancet *399*, 412-413.

Nettleship JE, Ren J, Rahman N, Berrow NS, Hatherley D, Barclay AN, Owens RJ. A pipeline for the production of antibody fragments for structural studies using transient expression in HEK 293T cells. Protein Expr Purif. 2008 Nov;62(1):83-9. doi: 10.1016/j.pep.2008.06.017. Epub 2008 Jul 10.

Nie J, Li Q, Wu J, Zhao C, Hao H, Liu H, Zhang L, Nie L, Qin H, Wang M. *et al*., (2020) Establishment and validation of a pseudovirus neutralization assay for SARS-CoV-2. Emerg Microbes Infect. *9*, 680-686.

Nutalai, R., Zhou, D., Tuekprakhon, A., Ginn, H., Supasa, P., Liu, C., Huo, J., Mentzer, A., Duyvesteyn, H.M.E., Dijokaite-Guraliuc, A., *et al.* (2022). Potent cross-reactive antibodies following Omicron breakthrough in vaccinees. Cell, published online: DOI: https://doi.org/10.1016/j.cell.2022.05.014.

Pinto, D., Park, Y.J., Beltramello, M., Walls, A.C., Tortorici, M.A., Bianchi, S., Jaconi, S., Culap, K., Zatta, F., De Marco, A., *et al.* (2020). Cross-neutralization of SARS-CoV-2 by a human monoclonal SARS-CoV antibody. Nature *583*, 290-295.

Sender, R., Bar-On, Y.M., Gleizer, S., Bernshtein, B., Flamholz, A., Phillips, R., and Milo, R. (2021). The total number and mass of SARS-CoV-2 virions. Proc Natl Acad Sci U S A *118*.
Sun, Y., and Ho, M. (2020). Emerging antibody-based therapeutics against SARS-CoV-2 during the global pandemic. Antib Ther *3*, 246-256.

Stewart SA, Dykxhoorn DM, Palliser D, Mizuno H, Yu EY, An DS, Sabatini DM, Chen IS, Hahn WC, Sharp PA, Weinberg RA, Novina CD. Lentivirus-delivered stable gene silencing by RNAi in primary cells. RNA. 2003 Apr;9(4):493-501. doi: 10.1261/rna.2192803. PMID: 12649500; PMCID: PMC1370415.

Stuart, D.I., Levine, M., Muirhead, H., and Stammers, D.K. (1979). Crystal structure of cat muscle pyruvate kinase at a resolution of 2.6 A. J Mol Biol *134*, 109-142.

Supasa, P., Zhou, D., Dejnirattisai, W., Liu, C., Mentzer, A.J., Ginn, H.M., Zhao, Y., Duyvesteyn, H.M.E., Nutalai, R., Tuekprakhon, A., *et al.* (2021). Reduced neutralization of SARS-CoV-2 B.1.1.7 variant by convalescent and vaccine sera. Cell *184*, 2201-2211 e2207.

Walls, A.C., Park, Y.J., Tortorici, M.A., Wall, A., McGuire, A.T., and Veesler, D. (2020). Structure, Function, and Antigenicity of the SARS-CoV-2 Spike Glycoprotein. Cell *181*, 281-292 e286.

Walls, A.C., Tortorici, M.A., Snijder, J., Xiong, X., Bosch, B.J., Rey, F.A., and Veesler, D. (2017). Tectonic conformational changes of a coronavirus spike glycoprotein promote membrane fusion. Proc Natl Acad Sci U S A *114*, 11157-11162.

Weinreich, D.M., Sivapalasingam, S., Norton, T., Ali, S., Gao, H., Bhore, R., Musser, B.J., Soo, Y., Rofail, D., Im, J., *et al.* (2021). REGN-COV2, a Neutralizing Antibody Cocktail, in Outpatients with Covid-19. N Engl J Med *384*, 238-251.

Winter G, Waterman DG, Parkhurst JM, Brewster AS, Gildea RJ, Gerstel M, Fuentes-Montero L, Vollmar M, Michels-Clark T, Young ID, Sauter NK, Evans G. DIALS: implementation and evaluation of a new integration package. Acta Crystallogr D Struct Biol. 2018 Feb 1;74(Pt 2):85-97. doi: 10.1107/S2059798317017235. Epub 2018 Feb 1. PMID: 29533234; PMCID: PMC5947772.

Wrapp, D., Wang, N., Corbett, K.S., Goldsmith, J.A., Hsieh, C.L., Abiona, O., Graham, B.S., and McLellan, J.S. (2020). Cryo-EM Structure of the 2019-nCoV Spike in the Prefusion Conformation. Science *367*, 1260-1263.

Yuan, M., Liu, H., Wu, N.C., Lee, C.D., Zhu, X., Zhao, F., Huang, D., Yu, W., Hua, Y., Tien, H., *et al.* (2020a). Structural basis of a shared antibody response to SARS-CoV-2. Science *369*, 1119-1123.

Yuan, M., Wu, N.C., Zhu, X., Lee, C.D., So, R.T.Y., Lv, H., Mok, C.K.P., and Wilson, I.A. (2020b). A highly conserved cryptic epitope in the receptor binding domains of SARS-CoV-2 and SARS-CoV. Science *368*, 630-633.

Yuan, M., Zhu, X., He, W.-T., Zhou, P., Kaku, C.I., Capozzola, T., Zhu, C.Y., Yu, X., Liu, H., Yu, W., *et al.* (2022). A broad and potent neutralization epitope in SARS-related coronaviruses. bioRxiv. https://doi.org/10.1101/2022.03.13.484037

Zahradnik, J., Marciano, S., Shemesh, M., Zoler, E., Harari, D., Chiaravalli, J., Meyer, B., Rudich, Y., Li, C., Marton, I., *et al.* (2021). SARS-CoV-2 variant prediction and antiviral drug design are enabled by RBD in vitro evolution. Nat Microbiol *6*, 1188-1198.

Zhou, D., Dejnirattisai, W., Supasa, P., Liu, C., Mentzer, A.J., Ginn, H.M., Zhao, Y., Duyvesteyn, H.M.E., Tuekprakhon, A., Nutalai, R., *et al.* (2021). Evidence of escape of SARS-CoV-2 variant B.1.351 from natural and vaccine-induced sera. Cell *184*, 2348-2361 e2346.

1052 Zhou, D., Duyvesteyn, H.M.E., Chen, C.P., Huang, C.G., Chen, T.H., Shih, S.R., Lin, Y.C.,
1053 Cheng, C.Y., Cheng, S.H., Huang, Y.C., *et al.* (2020). Structural basis for the neutralization of
1054 SARS-CoV-2 by an antibody from a convalescent patient. Nature structural & molecular
1055 biology *27*, 950-958.
1056

A

BA.1	A67V,Δ69-70,T95I,G142D,Δ143-145,N211I,Δ212,	ins214EPE
BA.1.1	A67V,Δ69-70,T95I,G142D,Δ143-145,N211I,Δ212,	ins214EPE
BA.2	T19I,Δ24-26,A27S, G142D,	V213G
BA.3	A67V,Δ69-70,T95I,G142D, Δ143-145,N211I,Δ212	
BA.4/5	T19I,Δ24-26,A27S, Δ69-70, G142D,	V213G

NTD

BA.1	G339D,	S371L,S373P,S375F,	K417N,N440K,G446S	
BA.1.1	G339D,R346K,	S371L,S373P,S375F,	K417N,N440K,G446S	
BA.2	G339D,	S371F,S373P,S375F,T376A,D405N,R408S,	K417N,N440K	
BA.3	G339D,	S371F,S373P,S375F, D405N,	K417N,N440K,G446S	
BA.4/5	G339D,	S371F,S373P,S375F,T376A,D405N,R408S,	K417N,N440K,	

RBD

BA.1	S477N,T478K,E484A,	Q493R,G496S,Q498R,N501Y,Y505H	
BA.1.1	S477N,T478K,E484A,	Q493R,G496S,Q498R,N501Y,Y505H	
BA.2	S477N,T478K,E484A,	Q493R,	Q498R,N501Y,Y505H
BA.3	S477N,T478K,E484A,	Q493R,	Q498R,N501Y,Y505H
BA.4/5	L452R,S477N,T478K,E484A,F486V,		Q498R,N501Y,Y505H

BA.1	T547K,D614G,H655Y,N679K,P681H,N764K,D796Y,N856K,Q954H,N969K,L981F			
BA.1.1	T547K,D614G,H655Y,N679K,P681H,N764K,D796Y,N856K,Q954H,N969K,L981F			
BA.2	D614G,H655Y,N679K,P681H,N764K,D796Y,			Q954H,N969K
BA.3	D614G,H655Y,N679K,P681H,N746K,D796Y,			Q954H,N969K
BA.4/5	D614G,H655Y,N679K,P681H,N764K, D796Y,			Q954H,N969K

B

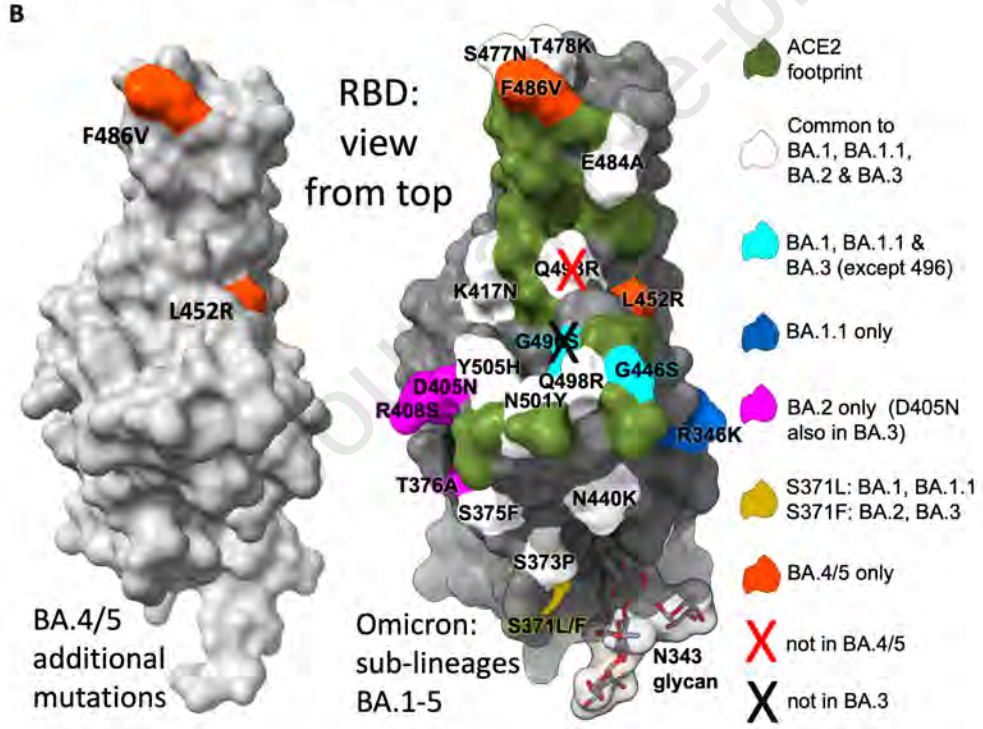

Figure 1

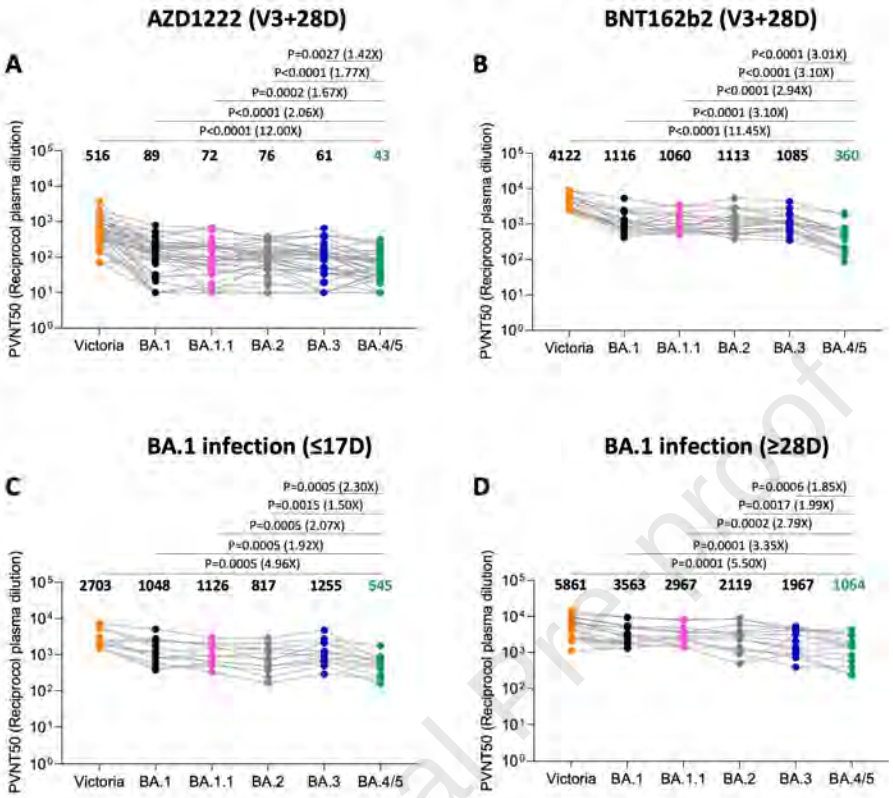

Figure 2

	IC50 (μg/mL)					
	Pseudoviruses					
mAbs	Victoria	BA.1	BA.1.1	BA.2	BA.3	BA.4
Omi-2	0.002	0.004	0.004	0.003	0.019	10
Omi-3	0.003	0.005	0.003	0.008	0.022	0.017
Omi-6	0.007	0.017	0.139	0.039	0.696	10
Omi-8	0.008	0.003	0.002	0.114	0.032	0.086
Omi-9	0.006	0.005	0.005	0.008	0.017	0.166
Omi-12	0.006	0.002	0.002	0.003	0.006	0.429
Omi-16	0.014	0.012	0.011	0.034	0.111	0.029
Omi-17	0.023	0.018	0.022	0.06	0.123	0.028
Omi-18	0.008	0.002	0.002	0.005	0.006	0.005
Omi-20	0.009	0.006	0.005	0.015	0.02	0.014
Omi-23	0.005	0.029	0.023	0.019	0.011	10
Omi-24	0.005	0.006	0.054	0.007	0.009	10
Omi-25	0.005	0.023	0.027	0.024	0.05	10
Omi-26	0.002	0.006	0.005	0.013	0.018	10
Omi-27	0.008	0.026	0.034	0.034	0.026	0.069
Omi-28	0.022	0.011	0.009	0.008	0.019	0.028
Omi-29	0.014	0.017	0.016	0.056	0.064	0.396
Omi-30	0.053	0.029	0.031	0.013	0.015	10
Omi-31	0.012	0.008	0.008	0.011	0.013	10
Omi-32	0.01	0.017	10	2.682	1.018	0.035
Omi-33	0.027	0.014	0.042	0.068	0.133	0.013
Omi-34	0.007	0.008	0.062	0.009	0.014	10
Omi-35	0.021	0.058	0.381	0.094	0.044	1.687
Omi-36	0.022	0.009	0.009	0.03	0.178	0.024
Omi-38	0.015	0.024	10	0.005	0.008	0.005
Omi-39	0.014	0.009	10	0.026	0.014	0.035
Omi-41	10	0.053	0.037	10	0.032	10
Omi-42	0.013	0.007	0.006	0.021	0.025	0.013
REGN10987	0.002	10	10	0.616	10	10
REGN10933	0.001	10	10	10	10	10
AZD1061	0.002	0.308	10	0.008	0.019	0.015
AZD8895	0.001	0.246	0.1	1.333	10	10
AZD7442	0.001	0.232	0.806	0.008	0.065	0.065
ADG10	0.007	10	10	10	10	10
ADG20	0.003	0.348	0.253	10	10	10
ADG30	0.014	10	10	10	10	10
Ly-CoV-555	0.002	10	10	10	10	10
Ly-CoV16	0.014	10	10	10	10	10
S309	0.13	0.094	0.138	0.638	0.228	1.041

Figure 3

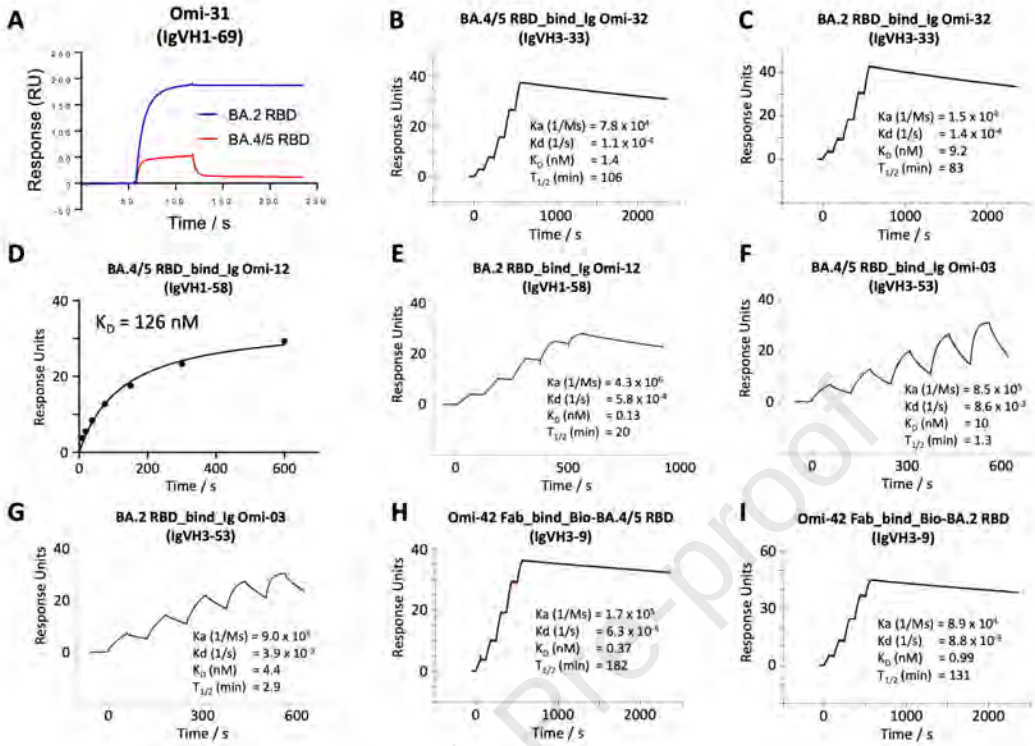

Figure 4

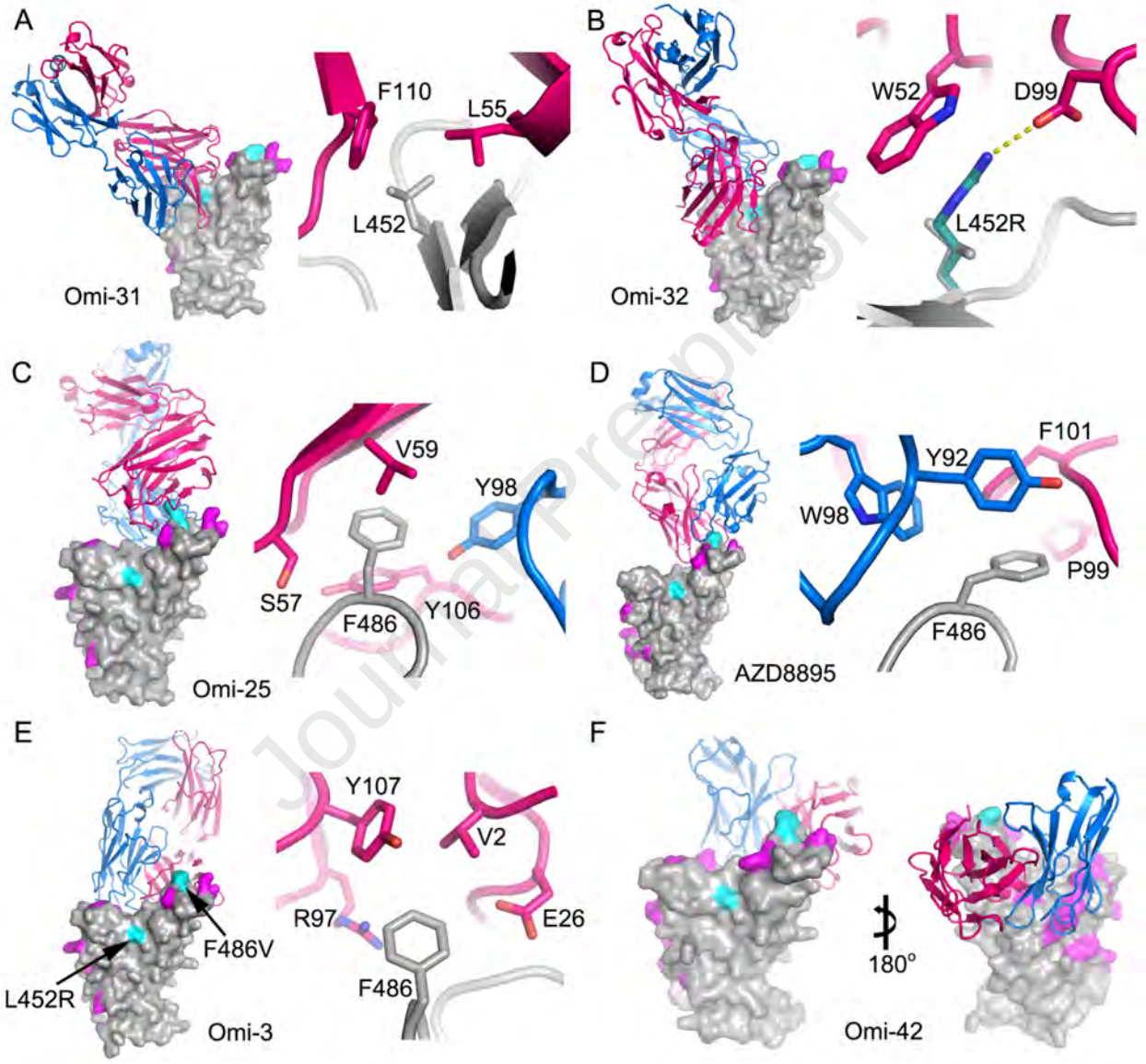
A
F110
L55
L452
Omi-31
B
W52
D99
L452R
Omi-32
C
V59
Y98
S57
F486
Y106
Omi-25
D
F101
Y92
W98
P99
F486
AZD8895
E
Y107
V2
R97
E26
F486
F486V
L452R
Omi-3
F
180°
Omi-42

Figure 5

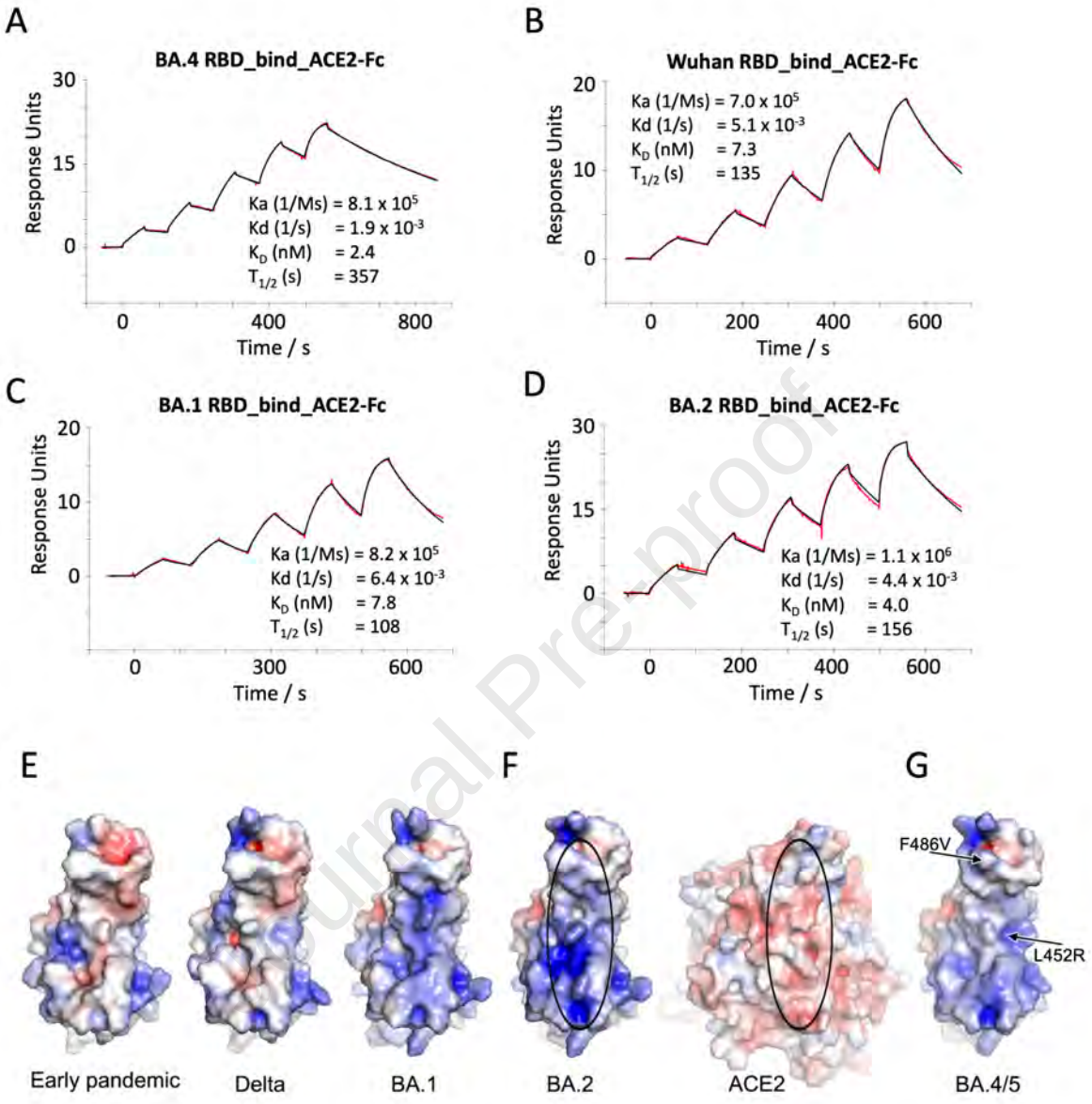
A
BA.4 RBD_bind_ACE2-Fc
Response Units
Time / s
Ka (1/Ms) = 8.1 x 10^5
Kd (1/s) = 1.9 x 10^-3
K_D (nM) = 2.4
T_1/2 (s) = 357
B
Wuhan RBD_bind_ACE2-Fc
Ka (1/Ms) = 7.0 x 10^5
Kd (1/s) = 5.1 x 10^-3
K_D (nM) = 7.3
T_1/2 (s) = 135
C
BA.1 RBD_bind_ACE2-Fc
Ka (1/Ms) = 8.2 x 10^5
Kd (1/s) = 6.4 x 10^-3
K_D (nM) = 7.8
T_1/2 (s) = 108
D
BA.2 RBD_bind_ACE2-Fc
Ka (1/Ms) = 1.1 x 10^6
Kd (1/s) = 4.4 x 10^-3
K_D (nM) = 4.0
T_1/2 (s) = 156
E
F
G
F486V
L452R
Early pandemic
Delta
BA.1
BA.2
ACE2
BA.4/5

Figure 6

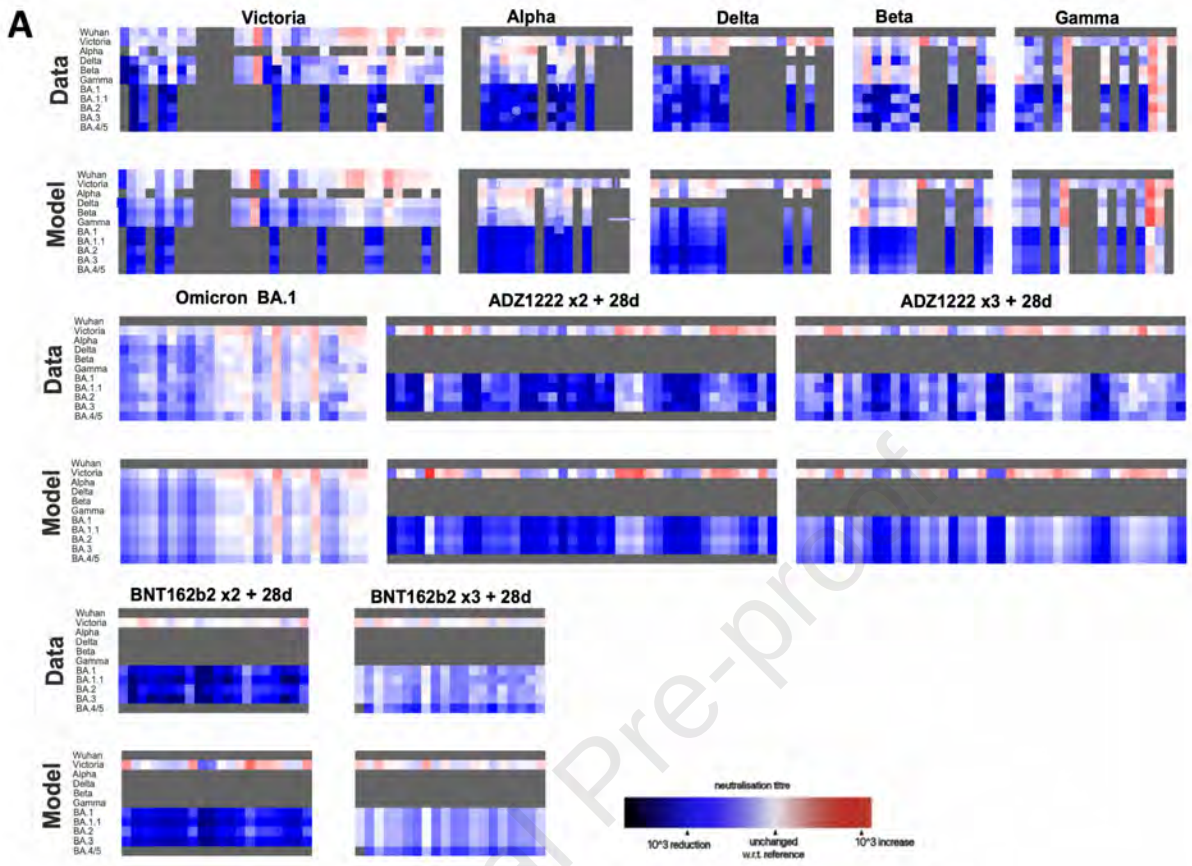
A
Victoria
Alpha
Delta
Beta
Gamma
Data
Model
Wuhan
Victoria
Alpha
Delta
Beta
Gamma
BA.1
BA.1.1
BA.2
BA.3
BA.4/5
Omicron BA.1
ADZ1222 x2 + 28d
ADZ1222 x3 + 28d
BNT162b2 x2 + 28d
BNT162b2 x3 + 28d
neutralisation titre
10^3 reduction
unchanged
w.r.t. reference
10^3 increase
B
Front view
Top view
Side view
BA.4/5
BA.1
BA.2
BA.3
Victoria
Wuhan
Gamma
Beta
Alpha
Delta

Figure 7

1. BA.4/5 resist neutralization by triple-dosed vaccinee serum more than BA.1/2.
2. BA.1 vaccine breakthrough serum shows reduced neutralization of BA.4/5.
3. Activity of SARS-CoV-2 therapeutic antibodies against BA.4/5 is reduced.
4. L452R and F486V mutations both make major contributions to BA.4/5 escape.

SARS-CoV-2 Omicron BA.4 and BA.5 sublineages bear mutations that lead to their reduced neutralization by sera from triple vaccinated individuals when compared to the more recent BA.1 and BA.2. Importantly, sera from individuals with breakthrough BA.1 infections also show reduced neutralization, suggesting that repeat Omicron infections are likely in the population.

.

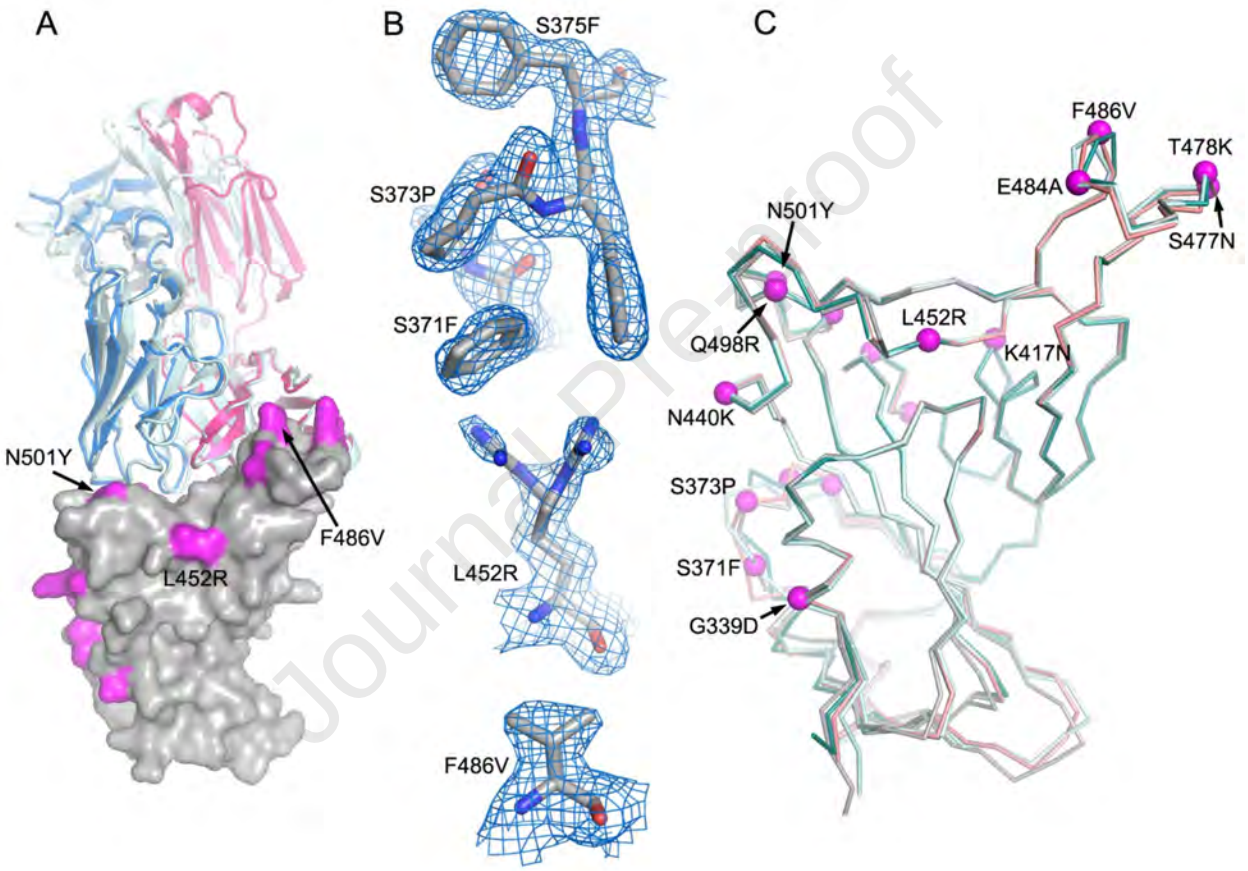

Figure S1

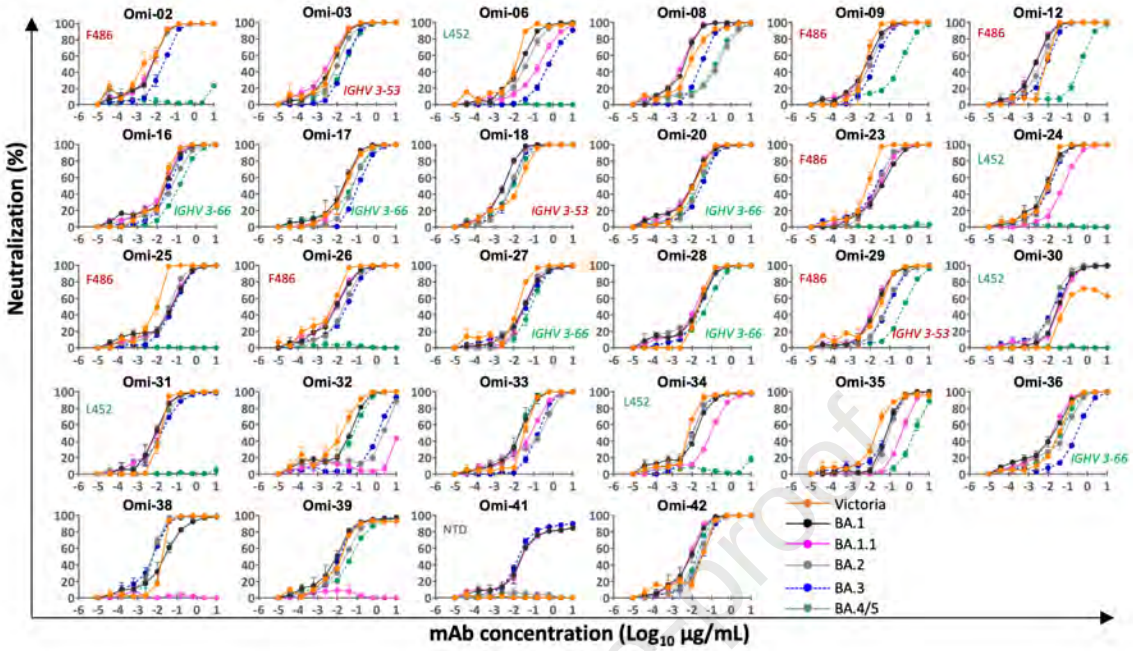

Figure S2

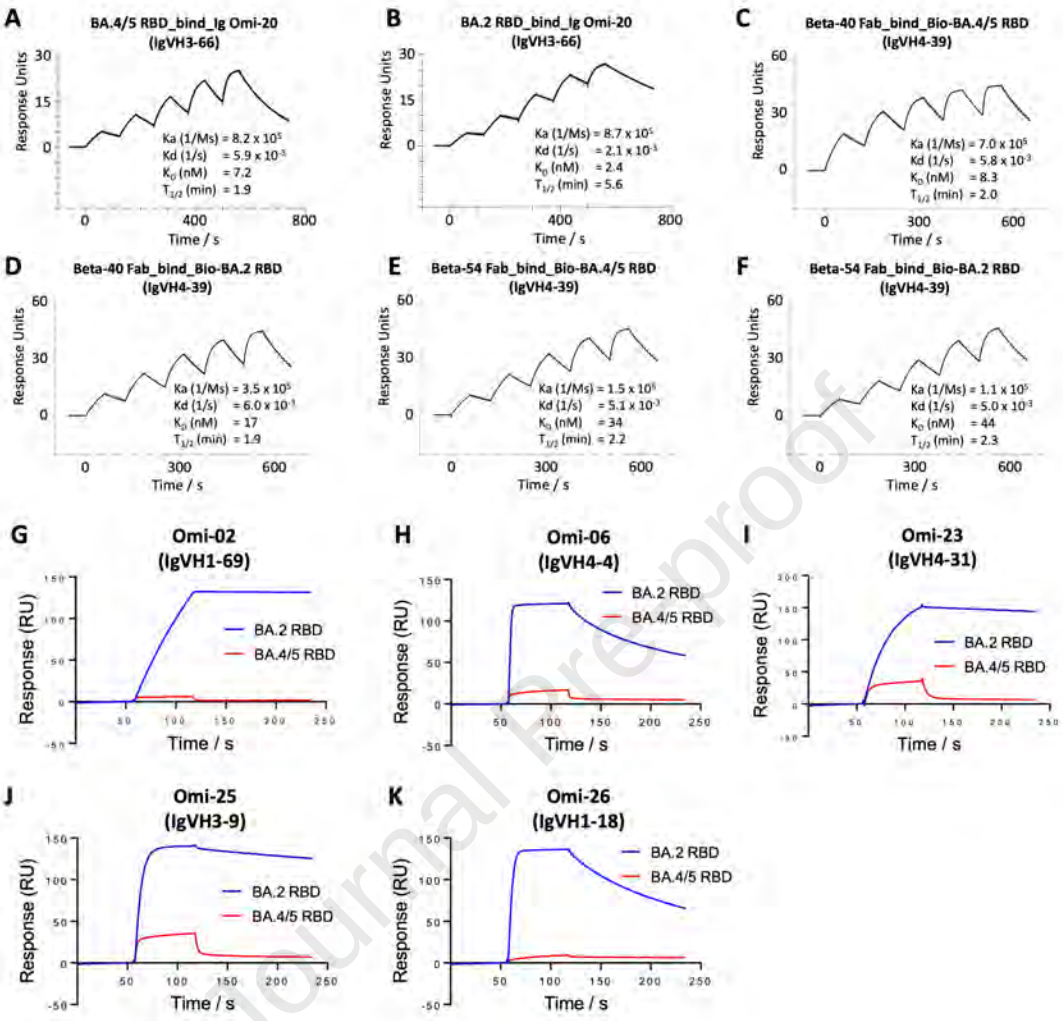

Figure S3

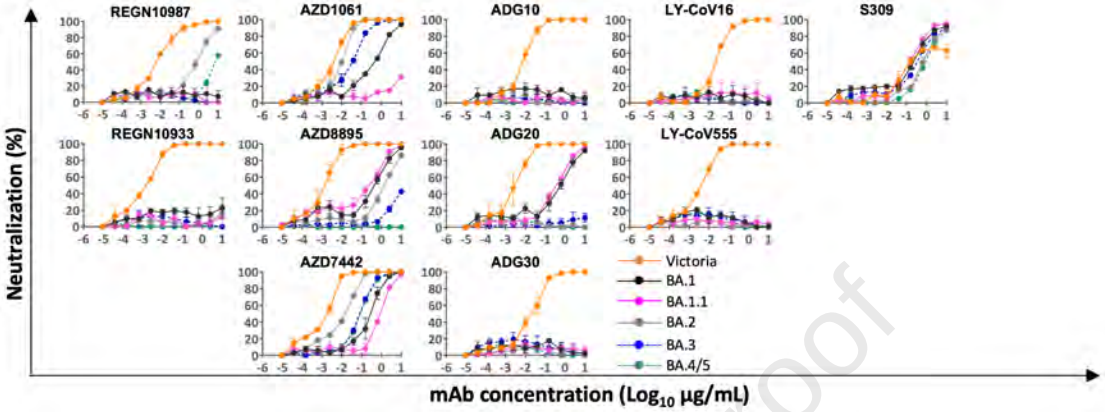

Figure S4

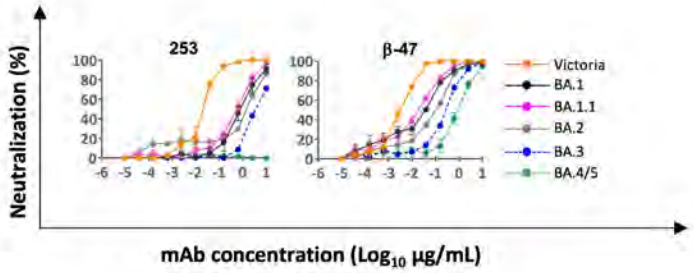

	IC50 (μg/mL)					
	Pseudovirus					
	Victoria	BA.1	BA.1.1	BA.2	BA.3	BA.4/5
mAb 253	0.021 ± 0.009	0.875 ± 0.373	0.415 ± 0.161	1.100 ± 0.049	7.523	>10
mAb β-47	0.003 ± 0.001	0.018 ± 0.009	0.011 ± 0.002	0.044 ± 0.006	0.169	0.807 ± 0.250

Figure S5

Table S1: Structure determination and refinement. Related to Methods.

Structure	**BA.4 RBD/Beta-27/NbC1, PDB: 7ZXU**
Data collection	
Space group	$P2_12_12_1$
Cell dimensions	
a, b, c (Å)	84.1, 100.4, 105.4
α, β, γ (°)	90, 90, 90
Resolution (Å)	66–1.89 (1.92–1.89)[a]
R_{merge}	0.313 (---)
R_{pim}	0.061 (0.848)
I/s(I)	7.7 (0.5)
$CC_{1/2}$	0.996 (0.418)
Completeness (%)	100 (99.4)
Redundancy	27.4 (28.2)
Refinement	
Resolution (Å)	66–1.89
No. reflections	68286/3756
R_{work} / R_{free}	0.183/0.210
No. atoms	
Protein	5805
Ligand/ion/water	672
B factors (Å^2)	
Protein	39
Ligand/ion/water	47
r.m.s. deviations	
Bond lengths (Å)	0.002
Bond angles (Å)	0.5

KEY RESOURCES TABLE

REAGENT or RESOURCE	SOURCE	IDENTIFIER
Antibodies		
Nanobody C1	Huo et al. 2020a	N/A
Fab	Dejnirattisai et al. 2021a	N/A
IgG	Dejnirattisai et al. 2021a and Liu et al 2021b	N/A
EY6A mAb	Zhou et al 2020	N/A
Regeneron mAbs	AstraZeneca	Cat#REGN10933, and REGN10987
AstraZeneca mAbs	AstraZeneca	Cat#AZD1061, AZD8895, and AZD7442
Vir mAbs	Adagio	Cat#S309
Lilly mAbs	Adagio	Cat#Ly-CoV555, and Cat#Ly-CoV16
Adagio mAbs	Adagio	Cat#ADG10, Cat#ADG20, and Cat#ADG30
28 mAbs generated from cases of Omicron breakthrough infection	Nutalai et al., 2022	N/A
Anti-c-Myc 9E10 antibody	Biolegend	Catt#626872
Bacterial, Virus Strains, and Yeast		
DH5α bacteria	InVitrogen	Cat#18263012
Saccharomyces cerevisiae EBY100	ATCC	Cat#MYA-4941
E. coli clone 10G cells	Lucigen, USA	Cat#60117-1
Biological Samples		
Serum from Pfizer-vaccinated individuals	University of Oxford	N/A
Serum from AstraZeneca-Oxford-vaccinated individuals	University of Oxford	N/A
Plasma from SARS-CoV-2 patients	John Radcliffe Hospital in Oxford UK, South Africa, and FIOCRUZ (WHO) Brazil	N/A
Chemicals, Peptides, and Recombinant Proteins		
His-tagged SARS-CoV-2 RBD	Dejnirattisai et al. 2021a	N/A
His-tagged SARS-CoV-2/Omicron RBD	This paper	N/A
His-tagged SARS-CoV-2/Omicron BA.4 RBD	This paper	N/A
His-tagged SARS-CoV-2/Omicron BA.5 RBD	This paper	N/A
His-tagged SARS-CoV-2 RBD-62	Zahradnik et al., 2021	N/A
His-tagged SARS-CoV-2 RBD N501Y	Supasa et al. 2021	N/A

His-tagged SARS-CoV-2 RBD K417N, E484K, N501Y	Zhou et al. 2021	N/A
His-tagged SARS-CoV-2 RBD K417T, E484K, N501Y	Dejnirattisai et al. 2021b	N/A
His-tagged SARS-CoV-2 RBD L452R, T478K	Liu et al. 2021a	N/A
His-tagged human ACE2	Liu et al 2021a	N/A
Human ACE2-hIgG1Fc	Liu et al. 2021a	N/A
His-tagged 3C protease	Libby et al. 1988	N/A
Phosphate buffered saline tablets	Sigma-Aldrich	Cat#P4417
Dulbecco's Modified Eagle Medium, high glucose	Sigma-Aldrich	Cat#D5796
Dulbecco's Modified Eagle Medium, low glucose	Sigma-Aldrich	Cat#D6046
FreeStyle™ 293 Expression Medium	Gibco	Cat#12338018
L-Glutamine–Penicillin–Streptomycin solution	Sigma-Aldrich	Cat#G1146
GlutaMAX™ Supplement	Gibco	Cat#35050061
Opti-MEM™	Gibco	Cat#11058021
Fetal Bovine Serum	Gibco	Cat#12676029
Polyethylenimine, branched	Sigma-Aldrich	Cat#408727
Strep-Tactin®XT	IBA Lifesciences	Cat#2-1206-025
HEPES	Melford	Cat#34587-39108
Sodium Chloride	Honeywell	Cat#SZBF3340H
LB broth	Fisher Scientific UK	Cat#51577-51656
Mem Neaa (100X)	Gibco	Cat#2203945
Trypsin-EDTA	Gibco	Cat#2259288
TrypLE™ Express Enzyme	Gibco	Cat#12604013
L-Glutamine 200 mM (100X)	Gibco	Cat#2036885
SYPROorange (5000X in DMSO)	Thermo	Cat#S6651
Isopropyl β-d-1-thiogalactopyranoside	Meridian Bioscience	Cat#BIO-37036
Kanamycin	Melford	Cat#K22000
Lysozyme	Sigma-Aldrich	Cat#L6876
Tris-base	Melford	Cat#T60040
Imidazole	Sigma-Aldrich	Cat#56750
Triton-X-100	Sigma-Aldrich	Cat#8787
Turbonuclease	Sigma-Aldrich	Cat#T4330
RNAse A	Qiagen	Cat#158922
NaCl	Sigma-Aldrich	Cat#S9888
MgSO4	Sigma-Aldrich	Cat#746452
Na2HPO4	Melford	Cat#S23100
NaH2PO4	Melford	Cat#S23185
HBS-EP+ Buffer 10×	Cytiva	Cat# BR100669
Regeneration Solution (glycine-HCl pH 1.7)	Cytiva	Cat# BR100838
Sensor Chip Protein A	Cytiva	Cat#29127555
Biotin CAPture Kit, Series S	Cytiva	CAT#28920234
His-tagged SARS-CoV-2 BA.1 variant RBD	This paper	N/A

His-tagged SARS-CoV-2 BA.2 variant RBD	This paper	N/A
SARS-CoV-2 BA.1 variant Spike	This paper	N/A
SARS-CoV-2 BA.2 variant Spike	This paper	N/A
Streptavidin-APC	Biolegend	Cat# 405207
Streptavidin-APC	Biolegend	Cat# 405207
RNase inhibitor	Promega	Cat# N2611
Protein G Plus/Protein A Agarose	Millipore	Cat#IP10
Pierce™ Fab Preparation Kit	Thermo Fisher	Cat#44985
Twin-Strep-tag® Capture Kit	IBA-Lifesciences	Cat# 2-4370-000
PEGRx 2	Hampton Research	HR2-084
ProPlex™ HT-96	Molecular Dimensions	MD1-42
JCSG-plus™ HT-96	Molecular Dimensions	MD1-40
Critical Commercial Assays		
Bright-Glo Luciferase Assay System	Promega	Cat# E2620
HIV Type 1 p24 Antigen ELISA 2.0	ZeptoMetrix	Cat# 0801002
Deposited Data		
Crystal structure of SARS-CoV-2 BA.4-RBD/Beta-27 Fab/Nanobody C1 complex	This paper	PDB: 7ZXU
Experimental Models: Cell Lines		
HEK293S GnTI- cells	ATCC	Cat#CRL-3022
HEK293 cells	ATCC	Cat#CRL-3216
Expi293F™ Cells	Gibco,	Cat#A14527
HEK293T/17 cells	ATCC	Cat#CRL-11268™
HEK293T cells	ATCC	Cat#CRL-11268
Hamster: ExpiCHO cells	Thermo Fisher	Cat#A29133
Recombinant DNA		
Vector: pHLsec	Aricescu et al., 2006	N/A
Vector: pNEO	Aricescu et al., 2006	N/A
Vector: pHLsec-SARS-CoV-2 spike of BA.1	This paper	N/A
Vector: pTTGneO-SARS-CoV-2 spike of BA.2	This paper	N/A
Vector: pTTGneO-SARS-CoV-2 RBD of BA.2	This paper	N/A
Vector: pNEO-SARS-CoV-2 RBD of BA.1	This paper	N/A
Vector: pCMV-VSV-G	Stewart SA et al. 2003	Addgene plasmid # 8454
pHR-SIN-ACE2	Alain Townsend	N/A
Vector: pOPING-ET	Nettleship et al., 2008	N/A
Vector: pJYDC1	Adgene	ID: 162458
Vector: p8.91	di Genova et al., 2020	Nigel Temperton
Vector: pCSFLW	di Genova et al., 2020	Nigel Temperton

Vector: pcDNA-SARS-CoV-2 spike of Wuhan strain	di Genova et al., 2020	Nigel Temperton
Vector: pcDNA-SARS-CoV-2 spike of Victoria strain (S247R)	Liu et al. 2021a	N/A
Vector: pcDNA-SARS-CoV-2 spike of Alpha strain (Δ69-70/144, N501Y, A570D, D614G, P681H, T716I, S982A, D1118H	Nutalai et al., 2022	N/A
Vector: pcDNA-SARS-CoV-2 spike of Beta strain (L18F, D80A, D215G, Δ242-244, R246I, K417N,E484K, N501Y, D614G, A701V)	Nutalai et al., 2022	N/A
Vector: pcDNA-SARS-CoV-2 spike of Gamma strain (L18F, T20N, P26S, D138Y, R190S, K417T, E484K, N501Y, D614G, H655Y, T1027I, V1176F)	Nutalai et al., 2022	N/A
Vector: pcDNA-SARS-CoV-2 spike of Delta+A222V strain (T19R, G142D, Del156-157/R158G, A222V, L452R, T478K, D614G, P681R, D950N)	Liu et al. 2021a	N/A
Vector: pcDNA-SARS-CoV-2 spike of BA.1 strain (A67V, Δ69-70, T95I, G142D/Δ143-145, Δ211/L212I, ins214EPE, G339D, S371L, S373P, S375F, K417N, N440K,G446S, S477N, T478K, E484A, Q493R, G496S, Q498R, N501Y, Y505H, T547K, D614G, H655Y, N679K, P681H, N764K, D796Y, N856K, Q954H, N969K, L981F)	Nutalai et al., 2022	N/A
Vector: pcDNA-SARS-CoV-2 spike of BA.1.1 strain (A67V, Δ69-70, T95I, G142D/Δ143-145, Δ211/L212I, ins214EPE, G339D, R346K, S371L, S373P, S375F, K417N, N440K,G446S, S477N, T478K, E484A, Q493R, G496S, Q498R, N501Y, Y505H, T547K, D614G, H655Y, N679K, P681H, N764K, D796Y, N856K, Q954H, N969K, L981F)	Nutalai et al., 2022	N/A
Vector: pcDNA-SARS-CoV-2 spike of BA.2 strain (T19I, Δ24-26, A27S, G142D, V213G, G339D, S371F, S373P, S375F, T376A, D405N, R408S, K417N, N440K, S477N, T478K, E484A, Q493R, Q498R, N501Y, Y505H, D614G, H655Y, N679K, P681H, N764K, D796Y, Q954H, N969K)	Nutalai et al., 2022	N/A

Vector: pcDNA-SARS-CoV-2 spike of BA.3 strain (A67V, Δ69-70, T95I, G142D/Δ143-145, Δ211/L212I, G339D, S371F, S373P, S375F, D405N, K417N, N440K, G446S, S477N, T478K, E484A, Q493R, Q498R, N501Y, Y505H, D614G, H655Y, N679K, P681H, N764K, D796Y, Q954H, N969K)	This paper	N/A
Vector: pcDNA-SARS-CoV-2 spike of BA.4/5 strain (T19I, Δ24-26, A27S, Δ69-70, G142D, V213G, G339D, S371F, S373P, S375F, T376A, D405N, R408S, K417N, N440K, L452R, S477N, T478K, E484A, F486V, Q498R, N501Y, Y505H, D614G, H655Y, N679K, P681H, N764K, D796Y, Q954H, N969K)	This paper	N/A
TM149 BirA pDisplay	University of Oxford, NDM (C. Siebold)	N/A
Software and Algorithms		
COOT	Emsley et al., 2010	https://www2.mrc-lmb.cam.ac.uk/personal/pemsley/coot/
Xia2-dials	Winter et al., 2018	https://xia2.github.io
PHENIX	Liebschner et al., 2019	https://www.phenix-online.org/
PyMOL	Warren DeLano and Sarina Bromberg	https://pymol.org/
Data Acquisition Software 11.1.0.11	Fortebio	https://www.fortebio.com/products/octet-systems-software
Data Analysis Software HT 11.1.0.25	Fortebio	https://www.fortebio.com/products/octet-systems-software
Prism 9.0	GraphPad	https://www.graphpad.com/scientific-software/prism/
IBM SPSS Software 27	IBM	https://www.ibm.com
mabscape	This paper	**Error! Hyperlink reference not valid.** https://snapcraft.io/mabscape
Biacore T200 Evaluation Software 3.1	Cytiva	www.cytivalifesciences.com
Flowjo 10.7.1	BD	https://www.flowjo.com
SnapGene software 5.3.2	Insightful Science	www.snapgene.com
Other		

X-ray data were collected at beamline I03, Diamond Light Source, under proposal ib27009 for COVID-19 rapid access	This paper	https://www.diamond.ac.uk/covid-19/for-scientists/rapid-access.html
TALON® Superflow Metal Affinity Resin	Clontech	Cat#635668
HiLoad® 16/600 Superdex® 200 pg	Cytiva	Cat#28-9893-35
Superdex 200 increase 10/300 GL column	Cytiva	Cat#28990944
HisTrap nickel HP 5-ml column	Cytiva	Cat#17524802
HiTrap Heparin HT 5-ml column	Cytiva	Cat#17040703
Amine Reactive Second-Generation (AR2G) Biosensors	Fortebio	Cat#18-5092
Octet RED96e	Fortebio	https://www.fortebio.com/products/label-free-bli-detection/8-channel-octet-systems
Buffer exchange system "QuixStand"	GE Healthcare	Cat#56-4107-78
Cartesian dispensing system	Genomic solutions	Cat#MIC4000
Hydra-96	Robbins Scientific	Cat#Hydra-96
96-well crystallization plate	Greiner bio-one	Cat#E20113NN
Crystallization Imaging System	Formulatrix	Cat#RI-1000
Sonics vibra-cell vcx500 sonicator	VWR	Cat#432-0137
Biacore T200	Cytiva	https://www.cytivalifesciences.com/en/us/shop/protein-analysis/spr-label-free-analysis/systems/biacore-t200-p-05644
QuixStand	GE Healthcare	Cat# 56-4107-78